Author Manuscript

Author Manuscript

Author Manuscript

Author Manuscript

HHS Public Access

Author manuscript

Nat Cell Biol. Author manuscript; available in PMC 2022 July 13.

Published in final edited form as:

Nat Cell Biol. 2022 January ; 24(1): 35–50. doi:10.1038/s41556-021-00822-7.

Cysteine Oxidation of Copper transporter SLC31A1/CTR1, drives VEGFR2 signaling and Angiogenesis

Archita Das[1,2], **Dipankar Ash**[1,3], **Abdelrahman Y. Fouda**[1,6,7], **Varadarajan Sudhahar**[1,2,6], **Young-Mee Kim**[1,3,9], **Yali Hou**[1,3,6], **Farlyn Z Hudson**[1,4], **Brian K Stansfield**[1,4], **Ruth B. Caldwell**[1,5,6], **Maggie McMenamin**[1,2,6], **Rodney Littlejohn**[1], **Huabo Su**[1], **Maureen R. Regan**[10,11], **Bradley J. Merrill**[10,11], **Leslie B. Poole**[8], **Jack H. Kaplan**[10], **Tohru Fukai**[1,2,6,#], **Masuko Ushio-Fukai**[1,3,#]

[1]Vascular Biology Center, Medical College of Georgia at Augusta University, Augusta, GA

[2]Departments of Pharmacology and Toxicology, Medical College of Georgia at Augusta University, Augusta, GA

[3]Department of Medicine (Cardiology), Medical College of Georgia at Augusta University, Augusta, GA

[4]Department of Pediatric, Medical College of Georgia at Augusta University, Augusta, GA

[5]Department of Cell Biology and Anatomy, Medical College of Georgia at Augusta University, Augusta, GA

[6]Charlie Norwood Veterans Affairs Medical Center, Augusta GA 30912

[7]Department of Pharmacology and Toxicology, University of Arkansas for Medical Sciences

[8]Department of Biochemistry, Wake Forest School of Medicine, University of Illinois College of Medicine, Chicago, Illinois 60607

[9]Department of Medicine (Cardiology), University of Illinois College of Medicine, Chicago, Illinois 60607

[10]Department of Biochemistry and Molecular Genetics, University of Illinois College of Medicine, Chicago, Illinois 60607

[11]Genome Editing Core, University of Illinois College of Medicine, Chicago, Illinois 60607

Users may view, print, copy, and download text and data-mine the content in such documents, for the purposes of academic research, subject always to the full Conditions of use: https://www.springernature.com/gp/open-research/policies/accepted-manuscript-terms

Address correspondence to: Masuko Ushio-Fukai, Ph.D, Vascular Biology Center, Department of Medicine, Cardiology, Medical College of Georgia at Augusta University, 1460 Laney-Walker Blvd, Augusta, GA 30912, USA, mfukai@augusta.edu; Tohru Fukai, MD, PhD, Vascular Biology Center, Dept of Pharmacology & Toxicology, Medical College of Georgia at Augusta University, 1460 Laney-Walker Blvd, Augusta, GA 30912, USA, tfukai@augusta.edu.

[#]equally contributed senior author

Author contributions

M.U.-F., T.F. and A.D. designed the study; A.D. (major), D.A., S.V., Y.H., Y.M.K., B.K.S., A.Y.F., R.B.C., F.Z.H., R.L. and H.S. performed/assisted research; M.U.-F., T.F., A.D. and Y.H., analyzed data; J.H.K., and L.B.P. discussed data and provided inputs; M.M. performed mouse genotyping; M.R.R. and B.M. generated the CRISPR/Cas9 knock-in mutant mice; J.H.K. and L.B.P. provided materials. M.U.-F., T.F. and A.D. wrote the manuscript; J.H.K. and L.B.P. edited the manuscript. All the authors reviewed the manuscript.

Competing financial interests

The authors declare no competing financial interests.

Author Manuscript Author Manuscript Author Manuscript Author Manuscript

Abstract

VEGFR2 (KDR/Flk1) signaling in endothelial cells (ECs) is essential for developmental and reparative angiogenesis. Reactive oxygen species (ROS) and copper (Cu) are also involved.in these processes. However, their inter-relationship is poorly understood. The role of endothelial Cu importer CTR1 in VEGFR2 signaling and angiogenesis *in vivo* is hitherto unknown. Here we show that CTR1 functions as a previously unrecognized redox sensor to promote angiogenesis in ECs. CTR1-depleted ECs showed reduced VEGF-induced VEGFR2 signaling and angiogenic responses. Mechanistically, CTR1 was rapidly sulfenylated at Cys189 in cytosolic C-terminus upon VEGF stimulation, which induced CTR1-VEGFR2 disulfide bond formation and their co-internalization to early endosomes, driving sustained VEGFR2 signaling. *In vivo*, EC-specific Ctr1-deficient mice or CRISPR/Cas9-generated "redox-dead" Cys to Ala Ctr1 knock-in mutant mice had impaired developmental and reparative angiogenesis. Thus, oxidation of CTR1 at Cys189 promotes VEGFR2 internalization and signaling to enhance angiogenesis. Our study uncovers an important mechanism for ROS sensing through CTR1 to drive neovascularization.

Vascular endothelial growth factor (VEGF) is a key angiogenic growth factor that stimulates migration, proliferation and capillary tube formation of endothelial cells (ECs), primarily through VEGF receptor type2 (VEGFR2/Flk1)[1]. VEGF binding to plasma membrane VEGFR2 induces receptor dimerization, autophosphorylation, and assembly of a membrane-proximal signaling complex. Endocytosis and subsequent receptor signaling from early endosomal compartments are major determinants of signaling output[2, 3]. Plasma membrane VEGFR2 interacts with Neuropilin 1[4], Ephrins[5], and Endophilin-A2[6], promoting VEGFR2 endocytosis and angiogenesis. Reactive oxygen species (ROS), especially H_2O_2, derived from NADPH oxidase (NOX) act as signaling molecules to promote angiogenesis in ECs and reparative neovascularization[7-16]. The signaling function of ROS acts through oxidation of cysteines (Cys) residues in proteins to generate "cysteine sulfenic acid (CysOH, sulfenylation)", which is involved in disulfide bond formation and redox signaling[17-19]. However, whether and how ROS regulate VEGFR2 endocytosis to activate VEGFR2 signaling remains elusive.

Copper (Cu) plays important roles in angiogenesis via unknown mechanisms [20-23]. Cellular Cu entry is mainly via the Cu transporter, CTR1 [24], which has one cytosolic Cys^{189} in the highly conserved C-terminal HCH^{190} triad [25] as well as key residues for Cu uptake such as Met-154 [26, 27]. We previously reported that mutation of the C-terminal triad, HCH^{190} to AAA^{190} accelerates Cu entry and also inhibits elevated Cu-induced CTR1 internalization (regulatory endocytosis) which protects cells against Cu toxicity[24, 25, 28, 29]. CTR1 is involved in Cu entry-dependent activation of MAPK signaling induced by growth factors such as FGF and insulin[30-32] and activation of Cu enzymes including lysyl oxidase (LOX)[33]. However, the role(s) of endothelial CTR1 in ROS-dependent VEGFR2 signaling as well as postnatal developmental and reparative angiogenesis *in vivo* are unknown.

In the present study, using various CTR1 mutant mice we show that endothelial CTR1 is a redox sensor, independent of its Cu transport function, which transmits the VEGF-induced ROS signal, via sulfenylation at Cys^{189} and subsequent disulfide bond formation between CTR1 and VEGFR2. The CTR1-VEGFR2 complex drives their co-internalization to activate

Author Manuscript Author Manuscript Author Manuscript Author Manuscript

endosomal sustained VEGFR2 signaling, which is required for developmental and reparative angiogenesis *in vivo*.

Results

Endothelial CTR1 is required for angiogenesis *in vivo*.

To address the role of CTR1 in angiogenesis *in vivo*, we examined CTR1 expression in developmental retina angiogenesis [34, 35] and mouse hindlimb ischemia (HLI) models [12, 13, 33]. Immunofluorescence analysis revealed that CTR1 colocalized with isolectin $B4^+$ ECs including tip cells in P5 postnatal developmental retina (Extended data Fig. 1A). Specificity of Ctr1 staining in ECs was confirmed by abolishing staining in ECs from inducible EC-specific Ctr1 knock out (KO)($Ctr1^{iECKO}$) mice, generated by crossing homozygous $Ctr1^{fl/fl}$ mice with mice expressing tamoxifen-inducible Cre recombinase under control of the VE-cadherin promoter (*VEcad-Cre-ERT2*)[36] (Extended Data Figs.1A and 1C). HLI model showed that CTR1 was colocalized with $CD31^+$ ECs and $Mac3^+$ macrophages in ischemic muscles at day 14 and day 3 after ischemia, respectively (Extended data Fig.1B). These results suggest that CTR1 is highly expressed in ECs in the developmental retina and reparative angiogenesis models.

To address the role of endogenous CTR1 in postnatal angiogenesis, we used mice carrying a single CTR1 allele ($Ctr1^{+/-}$). In the developmental retinal angiogenesis model, $Ctr1^{+/-}$ retina (P5) showed a slight but significant delay in vascular progression without affecting branching points and tip cells compared to WT retina (Extended Data Fig. 2A). In the skin wound healing model [37], $Ctr1^{+/-}$ mice exhibited a marked decrease in wound closure rate and $CD31^+$ capillary density in wounded tissues (Extended Data Fig 2B and 2C). In mouse HLI model, $Ctr1^{+/-}$ mice had no significant difference in blood flow recovery after ischemic injury, as compared to WT mice. We then performed bone marrow (BM) transplantation in $Ctr1^{+/-}$ mice to eliminate contributions of CTR1 in BM cells in reparative angiogenesis. Unexpectedly, lethally irradiated $Ctr1^{+/-}$ mice reconstituted with WT-BM, but not with $Ctr1^{+/-}$ BM, showed significant reduction of perfusion recovery and $CD31^+$capillary density in ischemic muscles, as compared to control group (WT mice reconstituted with WT-BM) (Extended Data Figs. 2D and 2E). Thus, CTR1 in tissue resident cells, but not BM cells, is required for reparative angiogenesis after HLI. Indeed, the role of CTR1 is tissue or cell-specific[38, 39].

To determine the role of endothelial CTR1 in postnatal angiogenesis *in vivo*, we used $Ctr1^{iECKO}$ mice (Extended Data Fig. 1C). Selective deletion of Ctr1 in ECs was validated by qPCR and western blot analysis in ECs, aorta and liver isolated from $Ctr1^{iECKO}$ and $Ctr1^{fl/fl}$ (control, wild type (WT)) mice (Extended data Fig.1D and 1E). We first used the retinal angiogenesis model to examine angiogenic sprouting in the mouse retina in P6 pups[34]. $Ctr1^{iECKO}$ mice showed a delayed expansion of the vascular plexus to the periphery with significant decrease in vascular length and the numbers of vascular branching points, tip cells, and filopodia in the sprouting region as compared to WT mice (Fig. 1A). Furthermore, the number of proliferating cells ($BrdU^+$) per endothelial field (Isolectin $B4^+$ cells) at the leading edge of the growing plexus (angiogenic front) were significantly decreased in

Author Manuscript Author Manuscript Author Manuscript Author Manuscript

$Ctr1^{iECKO}$ mice retinas (Fig. 1B). Thus, endothelial CTR1 controls vessel sprouting by promoting tip cell filopodial extension during developmental angiogenesis.

To address the role of endothelial CTR1 in reparative angiogenesis *in vivo*, we used the mouse HLI (Fig. 1C) and the skin wound healing models (Fig. 1D). Figure 1C shows that perfusion recovery and angiogenesis ($CD31^+$ capillaries) in response to HLI were significantly impaired in $Ctr1^{iECKO}$ mice. Figure 1D shows that $CTR1^{iECKO}$ mice exhibited a significant decrease in wound closure rate and $CD31^+$ capillary density in the wounded tissues compared to WT mice. We next examined the role of endothelial CTR1 in VEGF-mediated angiogenesis *in vivo* using ear angiogenesis models. Adenovirus encoding VEGF-A_{164} (Ad-VEGF) or β-gal was injected intradermally into the ear of $Ctr1^{iECKO}$ mice or WT mice to evaluate angiogenesis using whole-mount CD31 staining (Fig. 1E). We found that VEGF-induced and basal angiogenesis were significantly impaired in $Ctr1^{iECKO}$ mice compared to WT mice. These results suggest that endothelial CTR1 plays a critical role in developmental, VEGF-, ischemia- or wound injury-induced reparative angiogenesis.

CTR1 depletion blocks VEGF signaling and angiogenesis in ECs.

We next examined the role of CTR1 in VEGF-induced angiogenic responses in primary cultured ECs. The modified Boyden chamber assays showed that VEGF-induced EC migration was inhibited in HUVECs transfected with CTR1 siRNA (Fig. 2A and Extended Data Fig. 1F) or ECs isolated from $Ctr1^{iECKO}$ mice (mCtr1KO ECs) (Fig. 2D). Notably, CTR1 siRNA had no effect on EC migration induced by sphingosine 1-phosphate (S1P), another potent angiogenic agonist (Fig. 2A), supporting the specificity of CTR1 siRNA in VEGF-induced angiogenesis. Assays of capillary tube formation[40] showed that CTR1 depletion significantly inhibited the VEGF-induced increase in tube branch numbers and lengths on Matrigel and the number of sprouts in fibrin gel (Fig. 2B). We then examined the role of CTR1 in VEGF signaling in ECs. CTR1 depletion with siRNA significantly inhibited VEGF-induced p-MEK1/2, p-ERK1/2, p-p38MAPK and p-Akt levels without affecting their protein expression (Fig. 2C). Furthermore, mCtr1KO ECs showed almost complete inhibition of VEGF-induced signaling events (Fig. 2E). Since Cu entry is required for activating the Cu-dependent enzyme, LOX involved in angiogenesis [20-22, 33, 41, 42] and for Cu binding to MEK1/2, which increases p-ERK1/2 [32], we examined the role of Cu in VEGF-induced signaling. We found that a cell permeable Cu chelator, Tetrathiomolybdate (TTM) had no significant effects on VEGF-induced p-MEK1/2, p-ERK1/2, p-p38MAPK and p-Akt (Fig. 2F), as we previously reported[43]. The chelator efficacy was confirmed by the results that TTM greatly inhibited VEGF-induced LOX activity (Extended Data Fig. 3A) and $CuCl_2$-induced p-MEK1/2 and p-ERK1/2 in ECs (Extended Data Fig. 3B). Thus, CTR1 is involved in VEGFR2 angiogenic signaling in a way that is independent of its Cu transport function in ECs.

CTR1-Cys^{189}OH promotes VEGFR2 signaling and angiogenesis.

ROS, especially H_2O_2, derived from NOXes, including NOX4, play a critical role in VEGF signaling and angiogenesis in ECs and reparative neovascularization *in vivo*[8-16, 33]. Since CTR1 siRNA had no effects on VEGF-induced increase in DCF fluorescence, reflecting intracellular oxidation status, (Fig. 3A), we next examined whether CTR1 is a target of

Author Manuscript Author Manuscript Author Manuscript Author Manuscript

ROS, generated by VEGF. Since ROS production induces oxidation of Cys residues in target proteins to form CysOH (sulfenylation)[17-19] and CTR1 has an exposed Cys^{189} residue in its cytosolic C-terminus HCH^{190} triad (and one other distant transmembrane Cys^{161} residue), we examined if VEGF induces CysOH formation of CTR1 in ECs. A CysOH trapping probe, DCP-Bio1[19, 44] revealed that VEGF addition rapidly increased CysOH formation of CTR1 within 5 min, peaking at 30 min, which fell to basal levels within 4 h (Fig. 3B). In contrast, $CuCl_2$ addition to ECs did not induce CTR1-CysOH formation (Extended Data Fig 4). Importantly, VEGF-induced CTR1-CysOH formation was abolished by Nox4 knockdown (Fig. 3C), which inhibited VEGF-induced DCF fluorescence and angiogenic responses in ECs[10]. Furthermore, VEGF-induced CysOH formation of CTR1 was almost completely inhibited by adenovirus-expressing Flag-CTR1-C^{189}A, but not by Flag-CTR1-H^{190}A (negative control)(Fig. 3D). To examine the role of Nox4-dependent CTR1 Cys^{189} oxidation in VEGF signaling we transfected the CTR1-WT or CTR1-C^{189}A in Nox4-depleted ECs. Nox4 knockdown or overexpression of CTR1-C^{189}A or their combination inhibited VEGF signaling (p-MEK1/2, p-ERK1/2, p-p38MAPK, p-Akt) to a similar extent (Extended data Fig. 5A). These results suggest that CTR1 senses Nox4-derived H_2O_2 via thiol oxidation at Cys^{189}, which stimulates VEGF signaling in ECs.

We next examined the functional significance of CTR1-Cys^{189}OH formation for VEGF-induced angiogenic responses in ECs. Overexpression of CTR1-C^{189}A, but not CTR1-H^{190}A, inhibited VEGF-induced EC migration (Fig. 3F) or capillary network formation (Fig. 3G) without affecting ROS production (Fig. 3E and Extended data Fig. 5B and 5C), suggesting that it functions as a dominant negative. To demonstrate further the functional role of endogenous Cys oxidation of CTR1, we generated Cys oxidation-defective, “redox dead” mCtr1-C^{187}A (corresponding to human CTR1-C^{189}A) knock-in (KI) mutant (mCtr1-KI) mice using CRISPR-Cas9 genome editing (Fig. 3H, Extended data Fig. 6 and Methods). ECs isolated from $mCtr1^{KI/KI}$ mice ($mCtr1^{KI/KI}$ ECs) showed significant inhibition of VEGF-induced VEGFR2 signaling (Fig. 3I) and EC migration (wound scratch assay, Fig. 3J) as compared to WT-ECs.

Since other growth factors including FGF- and insulin, -induced ERK activation is CTR1-Cu transport-dependent[31, 32], we confirmed our TTM Cu chelator findings showing the Cu transport-independent VEGF-induced activation of MAPK, by re-expression of human (h)CTR1-M^{154}A (Cu transport defective), hCTR1-C^{189}A (Cys oxidation-defective) or hCTR1-WT in $CTR1^{-/-}$ MEFs transfected with hVEGFR2. We found that CTR1-C^{189}A almost completely inhibited VEGF-induced p-MEK1/2 and p-ERK1/2, while CTR1-M^{154}A had no effect (Figs. 4A), similar to the effects of TTM (Fig. 2F). In contrast, CTR1-M^{154}A, but not CTR1-C^{189}A, inhibited $CuCl_2$-induced phosphorylation of MEK1/2 and EKR1/2 (Fig. 4C), as also shown by TTM (Extended data Fig. 3B). Of note, TTM or CTR1-M^{154}A, but not CTR1-C^{189}A, also inhibited other growth factors (FGF and insulin)-induced p-ERK1/2 (Figs. 4E and 4F). Thus, VEGF-induced MAPK activation is CTR1 Cys^{189} oxidation-dependent but CTR1 Cu transport-independent, while Cu- or other growth factor-induced MAPK activation is Cu transport-dependent but CTR1 Cys^{189}-independent.

We next examined the specific roles of CTR1 Cys oxidation and its Cu transport function in VEGF-induced angiogenic responses by re-expression of hCTR1-WT, hCTR1-M^{154}A

Author Manuscript Author Manuscript Author Manuscript Author Manuscript

or hCTR1-$C^{189}A$ in CTR1-depleted bovine aortic ECs (BAEC) transfected with bovine siCTR1. CTR1-$C^{189}A$ completely inhibited VEGF-induced EC migration and capillary formation, while hCTR1-M^{154} partially blocked both VEGF-induced responses (Fig. 4B) presumably due to inhibiting Cu-dependent LOX activity involved in EC migration and capillary formation[33]. In contrast, $CuCl_2$-induced EC migration and capillary formation were completely inhibited by CTR1-$M^{154}A$, but not by CTR1-$C^{189}A$ (Fig. 4D and Extended data Fig. 7). Of note, CTR1-$C^{189}A$, but neither CTR1-$M^{154}A$ nor TTM, inhibited VEGF-induced EC proliferation that is mainly mediated through MAPK activation (Fig. 4B and Extended Data Figs. 3D and 7), but not through LOX activation (Extended data Fig. 3C). Thus, VEGF induces CTR1 Cys^{189} oxidation to promote VEGF signaling in a Cu transport-independent manner, in addition to the downstream Cu transport-dependent activation of the Cu-dependent enzyme LOX, which in turn stimulates angiogenic responses in ECs.

CTR1-$Cys^{189}OH$ promotes CTR1/VEGFR2 co-internalization.

To gain insight into the mechanism by which CTR1 promotes VEGFR2 signalling, we examined the role of CTR1 in VEGF-induced VEGFR2 internalization in ECs. Cell surface biotinylation assay revealed that VEGF addition promoted CTR1 internalization within 5 min which continued at least for 2 h, followed by returning to the cell surface within 4 h, all of which was co-temporaneous with VEGFR2 internalization and return (Fig. 5A and Extended data Fig 8A). We found that dynasore inhibited VEGF-induced CTR1 and VEGFR2 internalization (Extended Data Fig. 8B) and that VEGFR2 knockdown blocked VEGF-induced CTR1 internalization (Extended Data Fig. 8C), suggesting that VEGF-induced CTR1 endocytosis is dynamin- and VEGFR2-dependent. In contrast, $CuCl_2$ (25 μM), which did not induce CTR1 *Cys oxidation* (Extended Data Fig 4), rapidly promoted CTR1 internalization *without* affecting VEGFR2 (Extended Data Fig 8D). These results suggest that *Cu-induced*, *Cys oxidation-independent* CTR1 internalization (regulatory endocytosis) itself does not drive VEGFR2 internalization and that VEGF- and Cu-induced CTR1 internalizations are mediated through different mechanisms.

To elaborate the mechanism by which VEGF stimulation induces both CTR1 and VEGFR2 internalization, we examined the interactions between CTR1 and VEGFR2. Co-immunoprecipitation (Co-IP) assays showed that VEGF stimulation in ECs increased CTR1 binding to VEGFR2 within 5 min, which continued for at least 2 h (Fig. 5B). In contrast, CTR1 did not bind to VEGFR1 or VEGFR3 (Fig. 5B), suggesting that CTR1 interacts specifically with VEGFR2 in ECs. CTR1-VEGFR2 binding, was further confirmed by bimolecular fluorescence complementation (BiFC) assays[40, 45] which showed that co-transfection of Venus-N-terminal vector expressing CTR1 (CTR1-VN) and Venus-C-terminal vector expressing VEGFR2 (VEGFR2-VC) induced yellow fluorescent protein (YFP) fluorescence in cells stimulated with VEGF (Fig. 5C). In contrast, cells transfected with CTR1-VN and VC-expressing scrambled peptide (negative control) exhibited no fluorescence (Fig. 5C). This suggests that CTR1 directly interacts with VEGFR2 in response to VEGF. To determine the subcellular localization of CTR1 and VEGFR2, we performed immunofluorescence co-localization analysis. We found that CTR1 and VEGFR2 partially co-localized at the plasma membrane in the basal state, and VEGF stimulation promoted their co-internalization to the perinuclear region, with Rab5- or EEA1-positive

Author Manuscript Author Manuscript Author Manuscript Author Manuscript

early endosomes, but not Rab7-positive late endosomes (Figs. 5D1 and 5D2). Thus, VEGF stimulation rapidly promotes CTR1 binding to VEGFR2 and their subsequent co-internalization to early endosomes, thereby activating VEGFR2 downstream signalling in ECs.

Cell surface biotinylation (Fig. 5E and Extended Data Figs. 9A and 9B), co-IP (Fig. 5F) or co-localization analysis (Figs. 5G1 and 5G2) showed that VEGF-induced internalization, colocalization of CTR1 and VEGFR2 or their binding were almost completely inhibited in ECs transfected with CTR1-C^{189}A, as compared to CTR1-WT or CTR1-H190A. Thus, VEGF-induced CTR1-Cys^{189}OH is required for forming the CTR1-VEGFR2 complex, promoting their co-internalization. To address how CTR1-Cys^{189}OH promotes association with VEGFR2, we examined if CTR1-VEGFR2 forms intermolecular disulfide bonds (Fig. 6A). Co-IP assays in ECs transfected with Flag-hCTR1 and HA-hVEGFR2 in non-reducing gels showed that VEGF stimulated disulfide bond formation between CTR1 and VEGFR2 (Fig. 6A). To identify the Cys residues of VEGFR2 involved in CTR1-VEGFR2 complex formation, we made the VEGFR2 mutants in which highly conserved redox-sensitive Cys residues in C-terminus (Cys^{1201} or Cys^{1208} or $Cys^{1201,1208}$) [46] were mutated to Ala (Fig. 6B). Co-IP experiments revealed that CTR1-WT, but not CTR1-Cys^{189}A, bound to both VEGFR2-WT and VEGFR2-Cys^{1201}S, but not either VEGFR2-Cys^{1208}S or VEGFR2-$Cys^{1201,1208}$S variants, in response to VEGF (Fig. 6C). Importantly, the VEGFR2 variant-Cys^{1208}S, but not Cys^{1201}S, inhibited VEGF-induced VEGFR2 signaling (Fig. 6D) and EC angiogenic responses (Fig. 6E), as compared to VEGFR2-WT. These findings suggest that VEGF-induced CTR1-Cys^{189}-SOH binds to and reacts with VEGFR2 at Cys^{1208} to form an intermolecular disulfide bonded complex, which drives VEGFR2 signaling and EC angiogenic responses.

mCTR1-C^{187}A KI mice exhibit deceased angiogenesis *in vivo*.

To determine the role of endogenous CTR1 Cys oxidation in developmental and reparative angiogenesis *in vivo*, we used the Cys^{189} oxidation-defective “redox dead” mCtr1-$C^{187}A^{KI}$ mutant ($mCtr1^{KI}$) mice, as described in Fig. 3H and Extended Data Fig. 6. We found that both heterozygous $mCtr1^{KI/+}$ and homozygous $mCtr1^{KI/KI}$ mice had no phenotype in embryogenesis, they were viable and had normal body weight (Extended data Fig. 6C) and maintained the Mendelian ratio at birth. To assess the role of CTR1-Cys^{189} in postnatal developmental angiogenesis, we analyzed retinal angiogenesis in P5 pups and found that $mCtr1^{KI/KI}$ retinas showed a delayed expansion of the vascular plexus to the periphery with significant decrease in vascular length and the numbers of vascular branching points, tip cells, and filopodia in the sprouting region, as compared to WT retinas (Fig. 7A). Similarly, the vasculature of $mCtr1^{KI/+}$ retinas also showed delayed radial outgrowth but to a lesser extent than $mCtr1^{KI/KI}$ retinas. These results suggest the presence of gene dosage effects of inhibition of CTR1 Cys^{189} oxidation on postnatal developmental angiogenesis.

We next assessed role of CTR1-Cys oxidation in postnatal angiogenesis in adults. Aortic ring *ex vivo* assay on Matrigel showed that VEGF-induced vessel sprouting was significantly impaired in aorta from $mCtr1^{KI/KI}$ mice compared to WT mice (Fig. 7B). VEGF-induced ear (Fig. 7C) or retina angiogenesis (Fig. 7D) accessed by a whole-mount

Author Manuscript Author Manuscript Author Manuscript Author Manuscript

CD31 staining in adult mice injected with adenovirus encoding VEGF-A_{164} (Ad-VEGF) into the ear intradermally or the eye intravitreously, respectively, were significantly reduced in mCtr1$^{KI/KI}$ mice, as compared to WT mice. Basal angiogenesis in mice injected with Ad.LacZ showed no difference between WT and mCtr1$^{KI/KI}$ mice in both models (Figs. 7C and 7D). To examine further the role of endogenous CTR1 Cys oxidation in reparative postnatal angiogenesis *in vivo*, we performed the skin wound healing and HLI models. The mCtr1$^{KI/KI}$ mice exhibited a marked decrease in wound closure rate (Fig. 8A) as well as CD31^{+} capillary density in wounded tissues (Fig. 8B), as compared to WT mice. We confirmed that CTR1-CysOH formation was dramatically increased in wounded tissues of WT mice, which was completely abolished in mCtr1$^{KI/KI}$ mice (Fig. 8C). The HLI model showed that blood flow recovery as well as CD31^{+} capillary density and αSMA^{+} arteriogenesis were significantly decreased in mCtr1$^{KI/KI}$ mice, as compared to WT mice (Fig. 8D). BMT experiments revealed that lethally irradiated mCtr1$^{KI/KI}$ mice transplanted with WT-BM showed reduced limb perfusion recovery and CD31^{+} capillary density in ischemic muscles, as compared to control (WT mice reconstituted with WT-BM) (Extended Data Figs. 10A and 10B). These findings suggest that CTR1-Cys^{189} oxidation in tissue resident cells, but not BM cells, is required for ischemia-induced reparative neovascularization.

Discussion

Our work identifies a previously unrecognized function of CTR1 as a redox sensor that transmits the VEGF-induced H_2O_2 signal to promote VEGFR2 trafficking and signaling that is important in angiogenesis. VEGF stimulation induced sulfenylation of CTR1 at Cys^{189}, via NOX4, which promoted CTR1-VEGFR2 disulfide bond formation and their co-internalization to Rab5^{+} early endosomes required for sustained VEGFR2 signaling, postnatal developmental and reparative angiogenesis *in vivo*. Although $CuCl_2$ application to ECs induced CTR1 internalization (regulatory endocytosis) which is dependent on the HCH^{190} triad[24, 25, 28, 29], it did not induce internalization of VEGFR2 or CTR1-CysOH formation. Thus, our results strongly imply that VEGF- and Cu-induced CTR1 endocytosis are mediated through distinct mechanisms (in a Cys oxidation-dependent and -independent manner, respectively), and are involved in different functions, promoting angiogenesis and preventing Cu toxicity, respectively.

Global CTR1-deficient mice show early embryonic lethality (E8.5 to E9) [38, 47], while Ctr1$^{+/-}$ heterozygous mice are normal. [38, 47]. In this study, Ctr1$^{+/-}$ P5 retina had a very mild phenotype of angiogenic defects compared to Ctr1^{iECKO} retina. There was no significant difference in blood flow recovery between WT and CTR1$^{+/-}$ mice in HLI model. We thus performed BMT to eliminate the contribution of Ctr1$^{+/-}$ BM cells and found that CTR1 in tissue-resident cells including ECs, but not BM cells, plays an important role in reparative neovascularization. Indeed, the role of CTR1 is tissue or cell-specific[38, 39]. Our results suggest that gene dosage effects of global CTR1 deletion (Ctr1$^{-/-}$ vs. Ctr1$^{+/-}$ mice) in angiogenesis may be modulated by opposing (anti-angiogenic) effects of Ctr1$^{+/-}$ BM cells. The mCtr1-C^{187}A$^{KI/KI}$ mice have no phenotype in embryogenesis, which is consistent with previous reports that global KO or EC-specific KO for Nox4, which generates H_2O_2 in response to VEGF, are not embryonic lethal[7, 11, 48]. Thus, embryonic lethality due to global

Author Manuscript Author Manuscript Author Manuscript Author Manuscript

CTR1 deficiency might be mediated through effects other than Nox4-H_2O_2-meditated CTR1 Cys oxidation which is required for postnatal angiogenesis[7, 11, 48].

VEGFR2 has six highly conserved cysteine residues in the C-terminus and Cys^{1201} and Cys^{1208} are redox-sensitive (Fig. 6B), but $hCys^{1208}$ ($mCys^{1206}$) of VEGFR2 is a major Cys oxidation site for H_2O_2 [46]. Using Cys to Ser mutants of hVEGFR2, we showed that VEGFR2-Cys^{1208}S, but not VEGFR2-Cys^{1201}S, inhibited VEGF-induced CTR1-VEGFR2 complex formation, their co-internalization, and angiogenic responses in ECs, as compared to VEGFR2-WT. Thus, Cys^{1208} of VEGFR2 is required for intermolecular disulfide bond formation with CTR1-CysOH and their co-internalization. The proximity of VEGFR2 and CTR1 is supported by our previous observation that both are localized in plasma membrane caveolae/lipid rafts [49, 50]. It is shown that VEGFR2 signaling and internalization are regulated by several VEGFR2-binding co-receptors or proteins such as Ephrin B2[5], NUMB[51], and neuropilins[52]. We recently reported that the Cu transporting ATPase, ATP7A also binds to VEGFR2 to promote VEGFR2 signaling via limiting autophagic degradation of VEGFR2[43]. How the newly identified CTR1-VEGFR2 complex interacts with VEGFR2 binding proteins to facilitate internalization is worthy of future investigation.

Cu entry is involved in direct activation of MEK by Cu binding, stimulating phosphorylation of ERK[32], growth factor signaling by FGF and insulin, and activation of Cu enzyme LOX involved in angiogenesis [20-22, 33, 41, 42]. We found that VEGF-induced CTR1-Cys^{189}OH formation promotes phosphorylation of MEK1/2 and ERK1/2 in a Cu transport-independent manner in ECs. The Cu transport defective mutant, hCTR1-M^{154}A, or the Cu chelator TTM had no effect on VEGF-induced MAPK signaling, while they inhibited $CuCl_2$- and other growth factor (FGF and insulin)-induced responses. By contrast, the Cys oxidation-defective CTR1-C^{189}A inhibited VEGF-induced MAPK signaling without affecting $CuCl_2$- or growth factors-induced effects. These findings indicate that Cu-, FGF- and insulin-induced ERK activation is dependent on Cu transport by CTR1 but independent of the redox sensing by CTR1 Cys^{189} and that Cu transport-independent activation of MAPK by CTR1 is VEGF-specific.

The current findings are consistent with our previous reports that Cu uptake is dependent on CTR1 M^{154} [26, 27], but not the CTR1 HCH^{190} triad nor CTR1 C^{189}S mutant[25, 26]. Our results are in contrast to those by Tsai et al.[53], who measured the Cu content of HEK293Tcells after prolonged exposure to Cu (100μM for one hour), reporting that the Cys^{189} mutation reduced Cu entry. However, an earlier study measuring rates of tracer Cu uptake in Sf9 (insect) cells found that hCTR1-C^{189}S showed Cu transport with Km and Vmax values not lower than hCTR1-WT[26]. A similar study in HEK293T cells reported that truncations or mutations of C-terminal CTR1 HCH^{190} triad to AAA showed a higher Vmax and Km than hCTR1-WT [25, 24]. Earlier NMR studies of short CTR1 polypeptides concluded that Cys^{189} is essential for CTR1 trimerization[54]. However, since CTR1 following C-terminal HCH^{190} triad cleavage still transports Cu[24, 25], Cys^{189} seems not be essential for a trimerization of CTR1 required for Cu transport.

The present study also shows that TTM or CTR1-M^{154}A partially blocked VEGF-induced EC migration and tube formation without affecting EC proliferation, presumably due to

Author Manuscript Author Manuscript Author Manuscript Author Manuscript

inhibiting (Cu-dependent) LOX activity, which is required for VEGF-induced EC migration and tube formation, but not for EC proliferation. Furthermore, we found that co-internalized CTR1 (and VEGFR2) returned to the plasma membrane within 4hr after VEGF stimulation. Thus, cell surface CTR1 may subsequently activate Cu uptake-LOX axis-dependent angiogenic responses. These results suggest that redox-dependent modification of CTR1 which promotes Cu entry-*independent* activation of VEGFR2 signaling as well as the canonical Cu entry-*dependent* activation of Cu-dependent enzymes, such as LOX, are orchestrated to enhance angiogenic responses in ECs (Fig. 8E).

Our findings advance the understanding of how the ROS signal is sensed to promote VEGFR2 signaling and angiogenesis. Moreover, our results demonstrate an unexpected non-canonical role for thiol oxidation of the CTR1 at Cys^{189} as a vital link between Cu transport proteins, ROS-dependent VEGFR2 signaling and angiogenesis and provides insights into thiol-oxidized CTR1 as a potential new target for therapy in various angiogenesis-dependent diseases.

METHODS

Animal Study.

The animal protocols used in this study were approved by the institutional Animal Care Committee and institutional Biosafety Committee of Augusta University. All mice were maintained at the Augusta University animal facility. Room temperature and humidity were maintained at 22.5 °C and between 50% and 60%, respectively. All mice were held under the 12:12 (12-h light:12-h dark) light/dark cycle. Mice were held in individually ventilated caging with a maximum of 5 or a minimum of 2 mice per cage. 8 to 12 weeks old male and female mice were used for experiments.

Generation of inducible EC-specific CTR1 KO ($CTR1^{iECKO}$) mice:

Tamoxifen-inducible EC-specific CTR1 knockout ($CTR1^{iECKO}$) mice were generated by crossing $CTR1^{fl/fl}$ mice with VE-Cadherin (Cdh5)-ERT2 Cre mice[36] on a C57BL/6J background, which inactivates the CTR1 gene specifically in ECs upon tamoxifen administration. To induce postnatal deletion of endothelial CTR1 in adults, we administered tamoxifen (50 mg/kg of body weight) by i.p. injection into $CTR1^{fl/fl}$ (WT) or $CTR1^{fl/fl}$ / VEcad-ERT2 Cre mice. Injections were performed once per day for 10 days with 2 days break, followed by two weeks resting period to obtain $CTR1^{iECKO}$ mice. To induce deletion of endothelial CTR1 in pups, we administered tamoxifen (1 mg/ml, 50 μl) by i.p. injection to each pup from P2 to P4 and clearance and harvested at P6.

Generation of CRISPR (Cas-9) mediated mCtr1 $C^{187}A$ knock-in (KI) (corresponding to human CTR1 C189A) mice:

The *mCtr1* $C^{187}A$ mouse line was generated using Cas9 mRNA (TriLink bio #L6125100), sgRNA, and single-strand DNA homology-directed repair (HDR) method. The gRNA sequence (5'-TTGATATCAGACTCCACATA-3') was designed with MIT CRISPR design tool[55] to target the conserved $His\text{-}Cys\text{-}His^{188}$ motif at the C-terminal of mouse *mCtr1* gene (corresponding to the $His\text{-}Cys\text{-}His^{190}$ motif in human *CTR1* (*hCTR1*)). The single-stranded

Author Manuscript Author Manuscript Author Manuscript Author Manuscript

oligonucleotide (ssODN) incorporated *mCtr1* C187A mutation, was used as a template for CRISPR/Cas9-HDR mediated gene editing in wild type mice (C57BL/6). The sgRNA, Cas9 mRNA, and ssODN encoding m*Ctr1* C187A were then injected into the cytoplasm of mouse zygotes and viable two-cell stage embryos were transferred to pseudo-pregnant females by the transgenic core facility at University of Chicago (Fig. 3H, Extended data Fig 6). We analyzed the founders by a combination of PCR and next generation amplicon sequencing methods to detect the precise mutations and confirmed successful generation of *mCtr1* C^{187}A-KI mice. For genotyping offspring, we designed a PCR strategy sensitive enough to differentiate WT and m*Ctr1* C187A alleles that differ by 3 nt. One common forward primer was used for both alleles (5'- AGGCAGCAGATGCTGAGC-3'). The WT reverse primer (5'- TGTGGAGTCTGATATCAAT GGCA-3') is different from the m*Ctr1* C^{187}A KI reverse primer (5'-TGTGGAGTCT GATATCAATGAGC-3') by 3nt (underlined) on the 3' end. The PCR products were 223bp for WT and m*Ctr1* C^{187}A. For genotyping with next generation amplicon sequencing, a region flanking the C^{187}A mutation was PCR amplified with fluidigm adaptors and sequenced with the Illiumina miniSeq kit (FC-420-1002) then analyzed with the CRISPResso alignment program[56].

In vivo angiogenesis models:

All experiments were conducted at 8–12 week old male or female littermates of $CTR1^{fl/fl}$ (control, wild type (WT)) and $CTR1^{iECKO}$ mice or C57Bl6 (WT) and mCtr1-KI mice.

Hindlimb ischemia model.

Mice were subjected to unilateral hindlimb surgery under anesthesia with intraperitoneal administration of ketamine (87 mg/kg) and xylazine (13 mg/kg) as we reported[12, 13, 33]. Briefly, the left femoral artery was exposed, ligated both proximally and distally using 6-0 silk sutures and the vessels between the ligatures were excised. We measured ischemic (left)/ nonischemic (right) limb blood flow ratio using a laser Doppler blood flow (LDBF) analyzer (PeriScan PIM 3 System; Perimed).

Mouse skin wound healing model.

The backside skin of the mice was wounded using a 3-mm punch, and the wound diameters were measured using Image J software (v 1 .52) to determine the wound closure rate as reported[37]

Mouse ear angiogenesis assay.

Adenovirus encoding $VEGF_{164}$ (1×10^9 pfu) or Ad-LacZ (control) was intradermally injected into the right and left ear skin of adult mice, respectively as reported[57]. Five days after viral injection, animal was transcardially perfused with PBS and 4% paraformaldehyde (PFA) and processed as previously described[57]. The ears were stained with anti-CD31 to visualize the vascular network.

Mouse retinal angiogenesis assay.

Eyes from postnatal day 5 and day 6 pups mice were fixed in 4% paraformaldehyde for 30 min. Retinas were dissected and permeabilized overnight in PBS containing 1% BSA

Author Manuscript Author Manuscript Author Manuscript Author Manuscript

and 0.5% Triton X-100. The permeabilized retinas were incubated with biotin-conjugated isolectinB4 (IB4) (20μg/ml, Sigma-Aldrich), followed by Alexa Fluor 488–conjugated streptavidin (Invitrogen Life Technologies) co-stained with or without ERG (EC marker) antibody, and whole mounts were photographed under a fluorescence microscope. The total length and number of branch points of IB4-positive vessels in the entire retina were quantified on composite high-magnification images using Image J software (v 1 .52). *In vivo* proliferation of ECs in retina was measured by the BrdU assay following intraperitoneal injection of 300 μg of BrdU (Sigma #B5002) per P6 pup that weights about 3gm and then co-stained with anti-BrdU antibody and IB4 antibody (n=6 per group), as reported [57, 58].

Antibodies:

Anti-CTR1 (the polyclonal antibody to hCTR1 was generated by immunization of rabbits with Cys_VSIRYNSMPVPGPNGTIL peptide (ABBIOTEC), 1:1000 for IB and 1:200 for IP, and abcam# 129067, 1:200), anti-Flag (Sigma # F7425, #3165, 1:1000), anti-HA (Origene, clone CB051 # TA180128, 1:1000), anti-VEGFR2 (CS # 2479, 1:1000), anti-VEGFR1 (abcam # 2350, 1:1000), anti-VEGFR3 (R&D # AF349, 1:1000), p-VEGFR2(1175) (CS # 3770, 1:1000), anti-Na/KATPase (Iowa # A6F, 1:2000), p-ERK1/2 (CS # 9101, 1:1000), ERK1/2 (CS # 9102, 1:1000), p-MEK1/2 (CS # 9121, 1:1000), MEK1/2 (CS # 9122, 1:1000), p-p38 (CS # 9211, 1:1000), P38 (Santa Cruz # 7972, 1:1000), p-Akt (CS # 9271, 1:1000), Akt (Santa Cruz # 8312, 1:1000), anti-Tubulin (Santa Cruz # 5286, 1:1000), anti-Actin (Santa Cruz # 47778, 1:1000) and anti Rab5 (Santa Cruz # 46692, 1:500), anti Rab7 (Santa Cruz # 376362, 1:500), anti EEA1 (BD Bioscience # 610456, 1:500), anti CD31 (BD Biosciences # 550274, 1:200), Mac3 (BD Bioscience #550292, 1:200), Isolectin (Vector # B-1205, 1:200), and anti αSMA (Sigma # C6198, 1:200) antibodies were used. Secondary antibodies Goat Anti-Rabbit IgG-HRP conjugate (Bio Rad, #170-6515), Goat Anti-mouse IgG-HRP conjugate (Bio Rad, #170-6516), Alexa Fluor-488-goat anti rat IgG (Invitrogen, #A11006), Alexa Fluor-488-goat anti rabbit IgG (Invitrogen, #A11008), Alexa Fluor-546-goat anti mouse IgG (Invitrogen, #A11003) are used in a 1:2000 dilution.

siRNA and plasmids:

Human CTR1 silencer select pre-designed siRNA was purchased from Ambion # 4392420 and silencer negative control siRNA from Ambion #AM4611. Bovine CTR1 siRNA designed as sequence 5’GCUUUAAGAACGUGGAACU 3’ and 3’AGUUCCACGUUCUUAAAGC 5’ from Sigma. VEGFR2 siRNA purchased from Origene # SR302557. We received flag-hCTR1-WT from Dr. Jack Kaplan as a gift. We generated Flag-hCTR1-C^{189}A in which Cys^{189} is mutated to Ala^{189} or Flag-hCTR1-H^{190}A in which His^{190} is mutated to Ala^{190} (negative control) or Flag-hCTR1-M^{154}A in which Met^{154} is mutated to Ala^{154} by point mutation. The flag-CTR1-VN177 was constructed by cloning flag-hCTR1-WT (from the Kaplan lab) with Sal1/BamH1 sites into pFlagVN173N plasmid while the HA-VEGFR2-VC155 was constructed by cloning VEGFR2 with EcoR1/ Xho1 sites into pHA-VC155N plasmid[40, 45]. We purchased HA-hVEGFR2 plasmid from Sino Biological Inc # HG10012-CY. We generated HA-hVEGFR2-C^{1201}S, HA-hVEGFR2-C^{1208}S and HA-hVEGFR2-$C^{1201/1208}$S by point mutation as previously reported[46, 59].

Author Manuscript Author Manuscript Author Manuscript Author Manuscript

Cell Culture and transfection:

The primary HUVECs (human Umbilical Vein Endothelial Cells) from Lonza (CC-2519, USA) were cultured in EndoGRO (EMD Millipore) supplemented with 5% fetal bovine serum (FBS, Atlanta Biological), and used for experiments until passage 6. The primary BAECs (Bovine aortic endothelial cells) from VEC technologies were cultured in DMEM (Gibco-BRL) with 10% FBS. HEK293T cells from ATCC and Ctr1WT and Ctr1KO immortalized MEFs cell lines (gift from Dr. Dennis Thiele) were cultured in DMEM (Gibco-BRL) with 10% FBS. Human recombinant VEGF (R&D Systems) was used at 20ng/ml for cell treatment. For siRNA transfection, HUVECs were transfected with 30nM siRNAs using Oligofectamine (Invitrogen, 12252011). For plasmid DNA transfection, cells were transfected with DNA (~6ug) using polyethylenimine (PEI, Polysciences, USA). For double transfection of siRNA and plasmid DNA, cells were transfected with siRNAs (30nM) and plasmid DNA (6ug for 100 mm dishes) using JetPRIME (Polyplus, USA). After transfection, cells were transferred to growth medium and incubated for 48 h at 37°C before experiments.

Isolation of primary mouse aortic ECs:

To isolate ECs from mice, the thoracic aorta was cut into 1 mm rings. Each aortic ring was opened and seeded onto a growth factor-reduced matrix with the endothelium facing down. The segments were cultured in EC growth medium containing (DMEM, 10% FBS, valine, penicillin/streptamycin heparin, gentamycin, Endomito) for about 4 days. The endothelial sprouting starts as early as day 2. The segments were then removed and the cells were cultured continually until they reached confluence. The ECs were harvested using neutral proteinase and cultured in EC growth medium for another two passages before experiments. [33]

Bone marrow transplantation (BMT).

BMT was performed as we previously reported[33, 40]. BM cells were isolated by density gradient separation. Recipient mice were lethally irradiated with 9.5 Gy and received an intravenous injection of 3 million donor BM cells 24 h after irradiation. As reported before transplantation efficiency has been validated[33] Hindlimb ischemia was induced at 6 to 8 weeks after BMT.

Capillary network formation assay.

The cells were starved with 0.5% FBS EndoGro medium overnight. 60,000 cells were seeded on a growth factor-reduced Matrigel (Corning)-coated 48 well plate and incubated for 6 h and then fixed with 4% paraformaldehyde for image acquisition, as we have reported [33, 40]. The capillary tube length, number of branch points, or branch length were measured using ImagePro or Image J software (v 1 .52).

Fibrin bead angiogenesis assay:

The capillary-like sprouting fibrin bead assay was performed with minor modifications [40]. Briefly, primary HUVEC and fibroblasts (ATCC) were exposed to M199 medium with 10% FBS. HUVEC were attached to dextran-coated Cytodex 3 beads (GE Healthcare Bio-

Author Manuscript Author Manuscript Author Manuscript Author Manuscript

Sciences, NJ) and embedded at 250 beads/well in 24-well plate in a fibrin clot. Fibroblasts were then seeded as a monolayer over the clot at 1.5×10^5 cells/well. Clots were cultured under standard conditions in EGM-2 medium and media was changed every day for 5-7 days. Bright field and fluorescent images were taken using the Celigo image cytometer (Nexcelom), and sprout number was quantified for 80-100 beads per experimental group. The number of sprouts was taken as the number of independent sprouts extruding from each bead and normalized to the number of beads counted.

Wound scratch cell migration Assay:

Confluent ECs were scraped using sterilized 10-μL pipette tips, washed with 0.1% serum media, and stimulated with 20 ng/ml of VEGF for 16 h, as previously described[60]. Images were captured immediately at 0 h and at 16 h after the wounding[60].

Modified Boyden chamber migration assay:

Modified Boyden Chamber assays were conducted in duplicate 24-well transwell chambers [33, 40, 60]. The upper insert (8-μm pores coated with 0.1% gelatin) containing HUVEC suspensions (5×10^4 cells) were placed in the bottom 24-well chamber containing fresh media with 0.2% FBS and stimulants. The chamber was incubated at 37°C for 8 h. The membrane was fixed and stained using Diff-Quick. Six random fields at × 200 magnifications were counted.

DCP-Bio1 assay to detect Cys-OH formed (sulfenylated) proteins:

To measure sulfenic acid (CysOH) formation (sulfenylation) of proteins, cells were lysed in degassed-specific lysis buffer [50 mM HEPES, pH7.0 at room temperature, 5 mM EDTA, 50 mM NaCl, 50 mM NaF, 1 mM Na_3VO_4, 10 mM sodium pyrophosphate, 5 mM Iodoacetamide (IAA), 100 μM DTPA, 1% Triton-X-100, protease inhibitor, 200 unit/mL catalase (Calbiochem), 200 μM DCP-Bio1 (KaraFast, USA)] and then DCP-Bio1-bound proteins were pulled down with streptavidin beads (Thermo scientific, USA) overnight at 4 °C. DCP-Bio1-bound CysOH formed, sulfenylated-proteins were determined by immunoblotting with specific antibodies, as reported [19, 40, 61].

Bimolecular Fluorescence Complementation (BiFC) Assay:

HEK293 cells were transfected with flag-CTR1-VN173- and HA-VEGFR2-VC155 or negative control peptide using PEI. The positive YFP signals showing interaction between CTR1 and VEGFR2 were taken by confocal microscopy, as reported[40, 45].

Detection of internalized and cell surface proteins using cell surface biotinylation assays:

To detect cell surface VEGFR2 and CTR1, HUVEC were starved overnight before being stimulated with 20 ng/ml of VEGF or $CuCl_2$ (25μM) at 37 °C or co-incubated with dynasore, a dynamin-associated endocytic inhibitor (200nM) with VEGF for 30 min to allow internalization of cell surface proteins. Then, cells were incubated with cell surface biotinylation reagent 1 mM EZ-Link Sulfo-NHS-LC-Biotin (Thermo Fisher Scientific) on ice for 30 min, washed with 50mM glycine followed by cell lysis with RIPA buffer and processed for streptavidin bead pull down. Cell surface biotinylated VEGFR2 and CTR1

Author Manuscript Author Manuscript Author Manuscript Author Manuscript

was measured by Western blotting with VEGFR2 or CTR1 or Na/K ATPase (cell surface marker) antibodies and quantified by NIH Image J software (v 1 .52). To detect internalized VEGFR2 and CTR1, HUVECs were incubated with 0.6 mM primaquine (MP Biomedicals) at 37°C for 10 min to block recycling during the internalization step. The cells were washed twice with PBS and labelled with EZ-Link Sulfo-NHS-SS-Biotin for 60 min. The excess biotin was removed by washing the cells with glycine in PBS with Ca^{2+} and Mg^{2+}. The cells were then incubated with 20 ng/ml VEGF and 0.6 mM primaquine at 37 °C. They were exposed twice to GSH buffer (50 mM glutathione, 75 mM NaOH, 75mM NaCl, 1 mM EDTA, 0.1% BSA, pH 9.0) on ice for 20 min to remove surface biotin. GSH was quenched by washing with 5 mg/ml ice-cold iodoacetamide in PBS. After an additional wash with ice-cold PBS, cells were lysed with RIPA buffer and processed for streptavidin bead pull down. Internalized biotinylated VEGFR2 and CTR1 were measured by Western blotting using VEGFR2 and CTR1 antibodies as reported[25, 28, 29, 57, 62] and quantified by NIH Image J software (v 1 .52).

Histology and immunohistochemistry.

Mice were sacrificed, and wounded skin tissues or gastrocnemius skeletal muscles were harvested, fixed with 4% PFA overnight at 4 °C, and followed by sucrose dehydration and OCT embedding [33, 37, 40]. Capillary density was determined in 5 μ m thick sections that were stained with anti-mouse CD31 antibody (BD Biosciences) followed by biotinylated anti-mouse IgG antibody (Vector Laboratories). For immunohistochemistry, we used R.T.U. Vectorstain Elite (Vector Laboratories) followed by DAB (Vector Laboratories). Immunofluorescence staining was performed with primary antibodies against, CD31 or αSMA. Secondary antibodies were Alexa Fluor 488 or 546-conjugated goat anti-rabbit IgG and goat anti mouse IgG (Invitrogen). In each experiment, DAPI (Invitrogen) was used for nuclear counter-staining. Images were taken using a fluorescence microscope (Keyence, BZ-X700) or an Axioscope microscope with a 20 objective. Microscopy images were acquired with axiovision 4.8.2 software, BZ-X Analyzer software and ZEN 2.3 software (Zeiss).

Western blot analysis and Immunoprecipitation assay:

Cells were lysed in buffer [50 mM HEPES (pH 7.4), 5 mM EDTA, 100 mM NaCl, 1% Triton X-100, protease inhibitors (10 μg/ml aprotinin, 1 mmol/L phenylmethylsulfonyl fluoride, 10 μg/ml leupeptin) and phosphatase inhibitors (50 mmol/L sodium fluoride, 1 mmol/L sodium orthovanadate, 10 mmol/L sodium pyrophosphate)]. Lysates with or without immunoprecipitation were used for Western blotting, as we reported [60, 61]. Western blot acquisition was performed using a ImageQuant TL 8.1 software.

LOX activity measurement:

LOX activity in cells was measured by a high-sensitivity fluorescence assay as described[33, 37]. Protein samples were incubated in the presence and absence of 500 μ mol/L specific LOX inhibitor BAPN at 37 °C for 30 min with final reaction mixture supplied by Amplite Fluorimetric Lysyl Oxidase Assay kit (AAT Bioquest) to the manufacturer's instruction. The reaction was stopped on ice, and differences in fluorescence intensity (540-nm excitation wavelength and 590-nm emission wavelength) between samples with and

Author Manuscript Author Manuscript Author Manuscript Author Manuscript

without BAPN were determined. Specific activity was determined by the ratio of activity to relative amount of protein.

Statistics and Reproducibility:

Data are presented as mean ± SEM. The statistical analysis was based on sample size (*n*), indicating the number of biologically independent experiments, biologically independent samples, biologically independent animals, individual cells or fields of view as described in detail in the respective figure legends. No statistical method was used to pre-determine the sample size. Each experiment was performed a minimum of three to make sure similar results are reproducible. No samples or animals were excluded from the analysis. All mice/samples were randomized before experiments. We performed blinded to group allocation during data collection and analysis. Data were compared between groups of cells and animals by unpaired two tailed Student *t*-test when one comparison was performed or by ANOVA for multiple comparisons. When significance was indicated by ANOVA, the Tukey post-hoc and Bonferroni multiple comparison analysis was used to specify between group differences. Values of *$p<0.05$, **$p<0.01$ and ***$p<0.001$ were considered statistically significant. Statistical tests were performed using Prism v8 (GraphPad Software, San Diego, CA).

Data Availability:

Source data are provided with this study. All data supporting the findings of this study are available from the corresponding author on reasonable request. Unprocessed blots have been provided for Figs 2c,e,f, 3b-d,i, 4a-b,e-f, 5a-b,e-f, 6a-c and 8c and extended data Figs 1c,e, 3b, 4, 5a,c, 7a, 8a-d and 9a-b. Source data have been provided for Figs. 1a-e, 2a-f, 3a-g, i-j, 4a-f, 5a,b,d2, e-g2, 6c-e, 7a-d and 8a-d and extended data Figs 1d,f, 2a-e, 3a-d, 4, 5a, 6c, 7b, 8a-d, 9a-b and 10a-b.

Author Manuscript
Author Manuscript
Author Manuscript
Author Manuscript

Extended Data

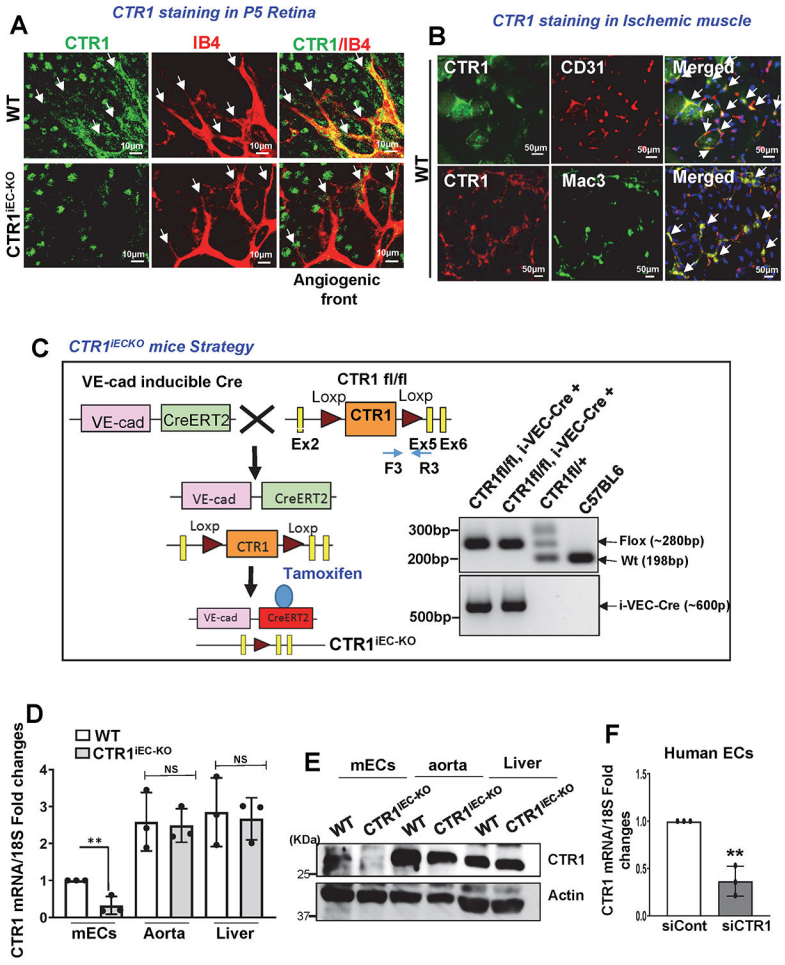

Extended Data Fig. 1. CTR1 expression in endothelial cells and characterization of inducible Endothelial CTR1-KO mice.

A. Co-staining for CTR1 and isolectin B4 (IB4) in a postnatal day (P)5 mouse retina in CTR1 WT and CTR1^{iECKO} mice in developmental retina angiogenesis models. Arrows indicate the tip sprouts of vessels. **B.** Co-staining for CTR1 and CD31 (EC marker) or Mac-3 (macrophage marker) and their colocalization (merged, white arrows) on day 3 (upper) and day 14 (lower), respectively, in ischemic gastrocnemius muscles in hindlimb ischemia models. Representative images from n=3 independent experiments are shown. **C.** Strategy to generate tamoxifen-inducible EC-specific CTR1 knockout (CTR1^{iECKO}) mice by crossing CTR1$^{flox/flox}$ mice with VE-Cadherin (Cdh5)-ERT2 Cre delete mice, which specifically express Cre in ECs upon tamoxifen administration. **D and E.** mRNA and proteins from aortic ECs, liver and lung isolated from WT and CTR1^{iECKO} mice and analyzed by qPCR and Western blotting using CTR1 antibody or Actin antibody (loading control) (n=6 biologically independent cells/samples), two-tailed unpaired t-test, **p= 0.0085. **F.** Real time qPCR analysis of CTR1 mRNA in HUVECs transfected with control or CTR siRNAs. (n=3 biologically independent experiments), two-tailed unpaired

t-test, **p= 0.0023. NS= not significant. Data are mean ± SEM). Source numerical data and unprocessed blots are available in source data.

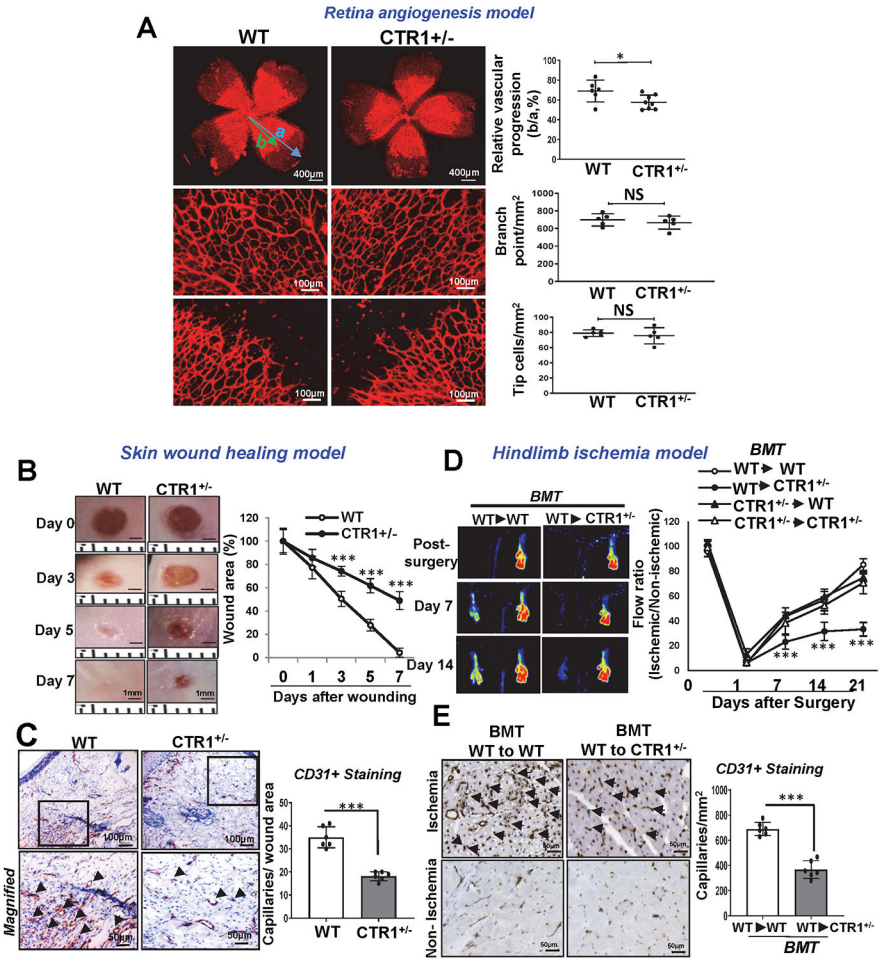

Extended Data Fig. 2. CTR1$^{+/-}$ mice show impaired postnatal developmental and reparative angiogenesis *in vivo*.

A. Retinal whole-mount staining with Isolectin B4 (IB4) of P5 WT and CTR1$^{+/-}$ mice. Right panels show quantification of vascular progression length, numbers of branch point and tip cells. (n=6 samples each for WT and CTR1$^{+/-}$, compared with Two-tailed unpaired t-test. *p=0.0378). **B and C.** WT and CTR1$^{+/-}$ mice were used for skin wound healing model. Representative images show time-course for wounded skin and graph represents the wound closure rates expressed as % of wound area from control at day 0 after wounding **(B).** Wounded tissues at day 7 were used to measure CD31^{+} capillary density **(C).** Boxes showed magnified images. Right panel showed the quantification. (n=6 mice per group, representative of two independent experiments, compared with two-way ANOVA followed by Bonferroni's multiple comparison analysis **(B)** or two-tailed unpaired t-test **(C)**). **D and E.** Irradiated WT or CTR1$^{+/-}$ mice were transplanted with bone marrow (BM) from WT or CTR1$^{+/-}$ mice. After 6 weeks of BM transplantation (BMT), mice were subjected to hindlimb ischemia and limb blood flow was measured at indicated days after surgery using a laser Doppler flow analyzer **(D).** In E, CD31^{+} capillary density (angiogenesis) in ischemic

Author Manuscript Author Manuscript Author Manuscript Author Manuscript

Author Manuscript Author Manuscript Author Manuscript Author Manuscript

and non-ischemic gastrocnemius muscles was measured at day 21 after surgery. (n=6 mice per group, representative of two independent experiments, compared with two-way ANOVA followed by Bonferroni's multiple comparison analysis **(D)**, or Two-tailed unpaired t-test **(E)**, ***p<0.001. NS=not significant. Data are mean ± SEM). Source numerical data are available in source data.

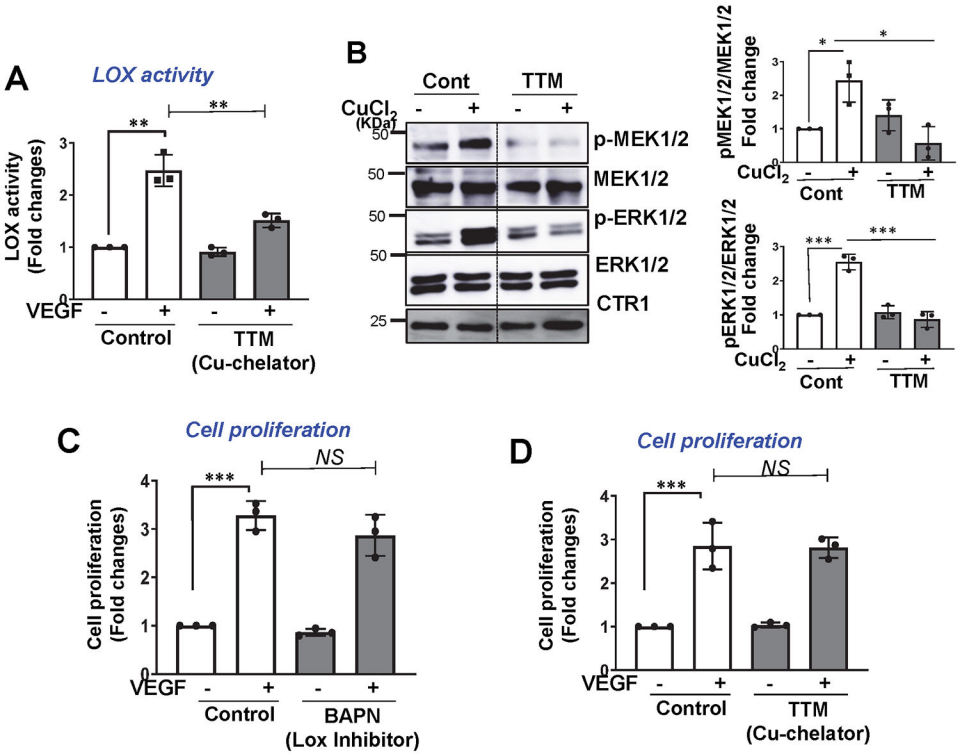

Extended Data Fig. 3. Cu-dependent LOX activity is not required for VEGF-induced EC proliferation.

A and **D.** HUVECs treated with Cu chelator, TTM (20nM) for 24hr were used to measure LOX activity in conditioned media (**A**) or cell proliferation measured by BrdU incorporation (**D**) after VEGF stimulation for 24 hr. **B.** HUVECs treated with Cu chelator TTM for 24 hr were stimulated with $CuCl_2$ (25μM) for 5 min, and lysates were used to immunoblotted (IB) with anti-p-MEK1/2 or p-ERK1/2 and their total proteins antibodies. **C.** HUVECs treated with specific LOX inhibitor, BAPN (100μM) for 24h were used to measure VEGF-induced cell proliferation as described. (n=3 biologically independent experiments). **A and B,** two-tailed unpaired t-test. **C and D,** one-way ANOVA followed by Tukey's multiple comparisons analysis, *p<0.05, **p<0.01, ***p<0.001. NS=not significant. Data are mean ± SEM. Source numerical data and unprocessed blots are available in source data.

Author Manuscript Author Manuscript Author Manuscript Author Manuscript

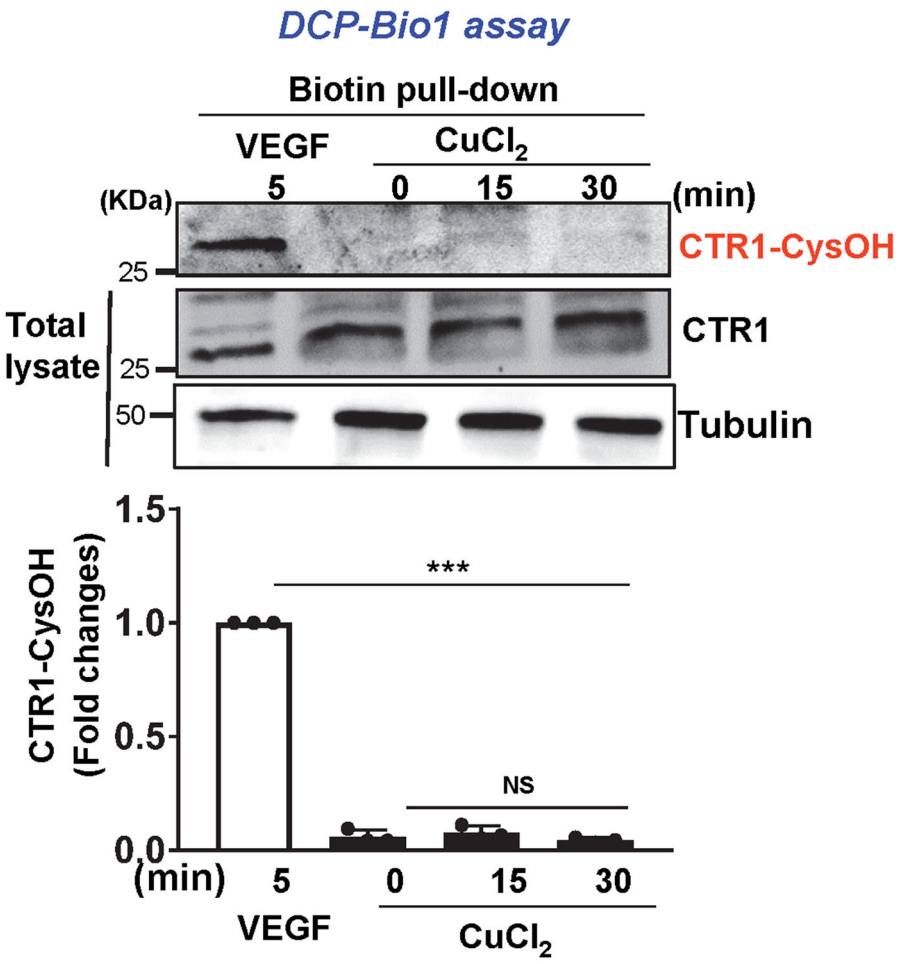

Extended Data Fig. 4. $CuCl_2$ does not induce CTR1 Sulfenylation.

HUVECs were stimulated with $CuCl_2$ (25μM) for indicated times or VEGF (20ng/ml) for 5min (for positive control), and DCP-Bio1-labeled lysates were pulled down with streptavidin beads and then IB with CTR1 or actin antibody to detect their CysOH formation. Bottom panel represents averaged CTR1-CysOH/total CTR1 level expressed by fold change from VEGF-induced CTR1-CysOH level as 1.0. (n=3 biologically independent experiments) two-tailed unpaired t-test. ***p<0.001. NS=not significant. Data are mean ± SEM. Source numerical data and unprocessed blots are available in source data.

Author Manuscript Author Manuscript Author Manuscript Author Manuscript

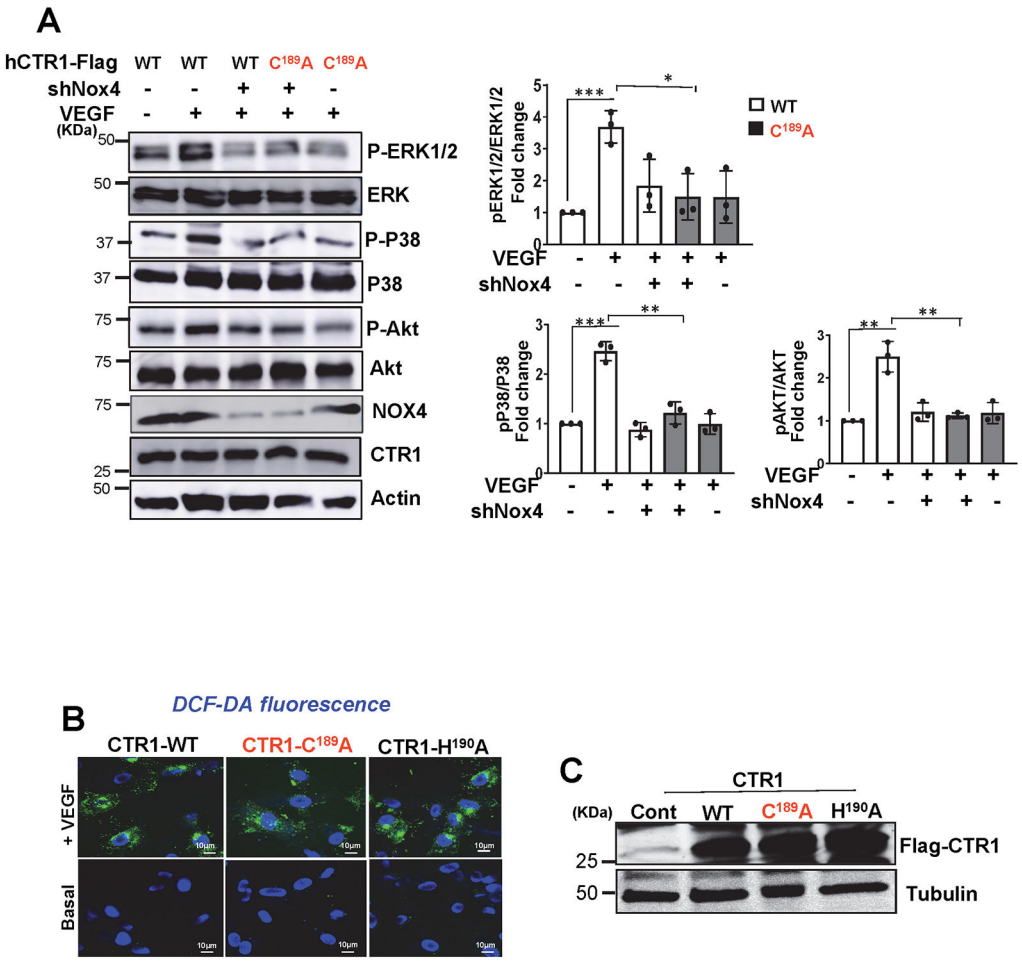

Extended Data Fig. 5. Nox4-ROS-CTR1 Cys^{189}OH axis is required for VEGF-induced VEGFR2 downstream signaling in ECs.

A, HUVECs transfected with Flag-hCTR1-WT, or Flag-hCTR1-C189A were infected with Ad.null (control) or Ad.shNox4 and stimulated with VEGF for 5 min to measure VEGF signaling using IB with antibodies indicated. Graphs represent the averaged fold change of phosphorylated proteins/total proteins over the basal control. (n=3 biologically independent experiments) two-tailed unpaired t-test. ***p= 0.0008, *p= 0.013, ***P= 0.0002, **P= 0.0019, **P= 0.0019, **P= 0.0028. Data are mean ± SEM. **B and C.** HUVECs transfected with Flag-CTR1-WT or Flag-hCTR1-C^{189}A or Flag-hCTR1-H^{190}A were stimulated with VEGF (20ng/ml) for 5min to measure DCF fluorescence with DAPI staining (**B**). In **C**, lysates were used for IB with Flag antibody to verify expression of transfected CTR1 proteins. Tubulin is a loading control. **B, C.** The experiment is representative of 3 independent experiments that yielded similar results. Source numerical data and unprocessed blots are available in source data.

Author Manuscript Author Manuscript Author Manuscript Author Manuscript

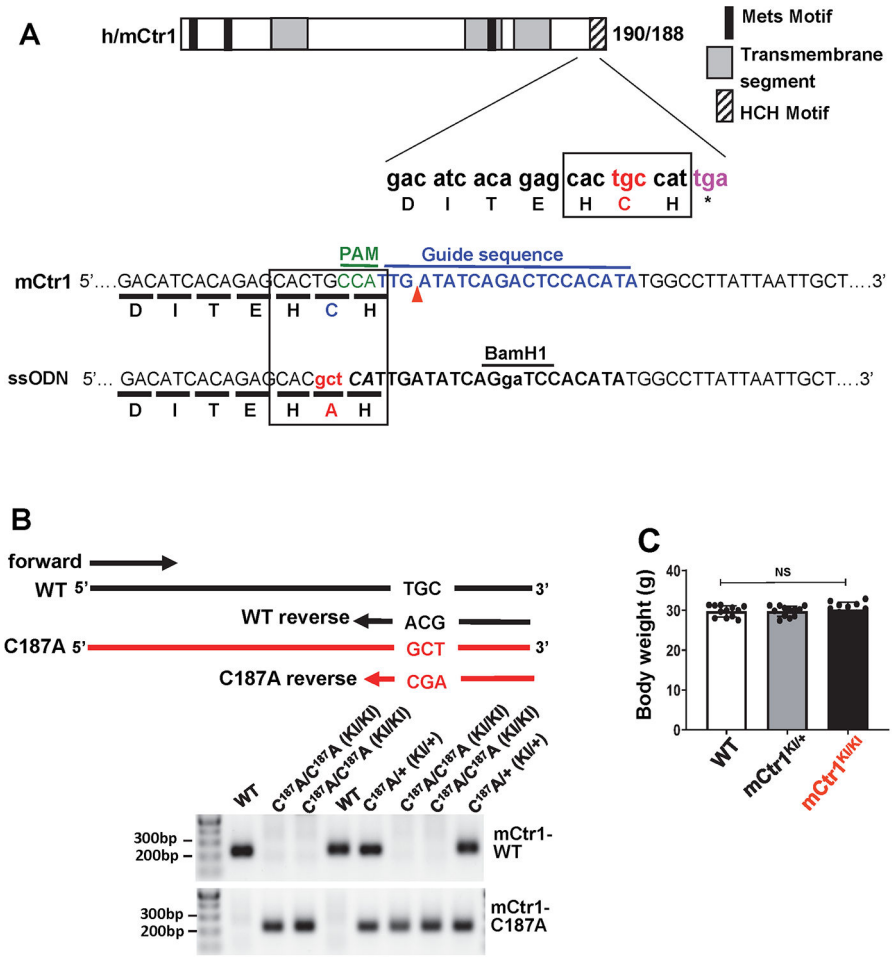

Extended Data Fig. 6. Generation of *Cys* oxidation defective "redox dead" mouse mCtr1-C187A (corresponding to human CTR1-C^{189}A) knock-in (KI) mutant (mCtr1-KI) mice by using CRISPR-Cas9 genome editing.

A. Alignment of partial amino acid sequences from human and mouse CTR1, indicating homology (boxes) between human Cys^{189} and mouse Cys^{187}. Schematic of the 20-nucleotide sgRNA target sequence of the mCtr1 (blue) and the PAM (green). The red arrowhead indicates the Cas9 cleavage site. ssODN, which contains 90 base pairs (bp) of homology sequence flanking each side of the target site was used as HDR template. ssODN incorporates point mutations (red) and BamHI restriction enzyme site (underlined by black). **B.** CTR1 CRISPR mice genotyping for mCtr1C^{187}A mutant and mCtr1WT after cross breeding with mCtr1$^{KI/+}$ and mCtr1$^{KI/+}$. Multiplex PCR genotyping of mCtr1 (C^{187}A) progeny. One common reverse primer was used for both genotypes. The PCR products were in between 300-200bp. HDR indicates homology directed repair; sgRNA, single-guide RNA; ssODN, single-strand oligoDNA. The experiment is representative of 6 independent experiments that yielded similar results. **C.** Body weight of WT, mCtr1$^{KI/+}$ and mCtr1$^{KI/KI}$ mice. (n=12 mice per group, compared with two-tailed unpaired t-test. NS= not significant. Data are mean ± SEM). Source numerical data are available in source data.

Author Manuscript Author Manuscript Author Manuscript Author Manuscript

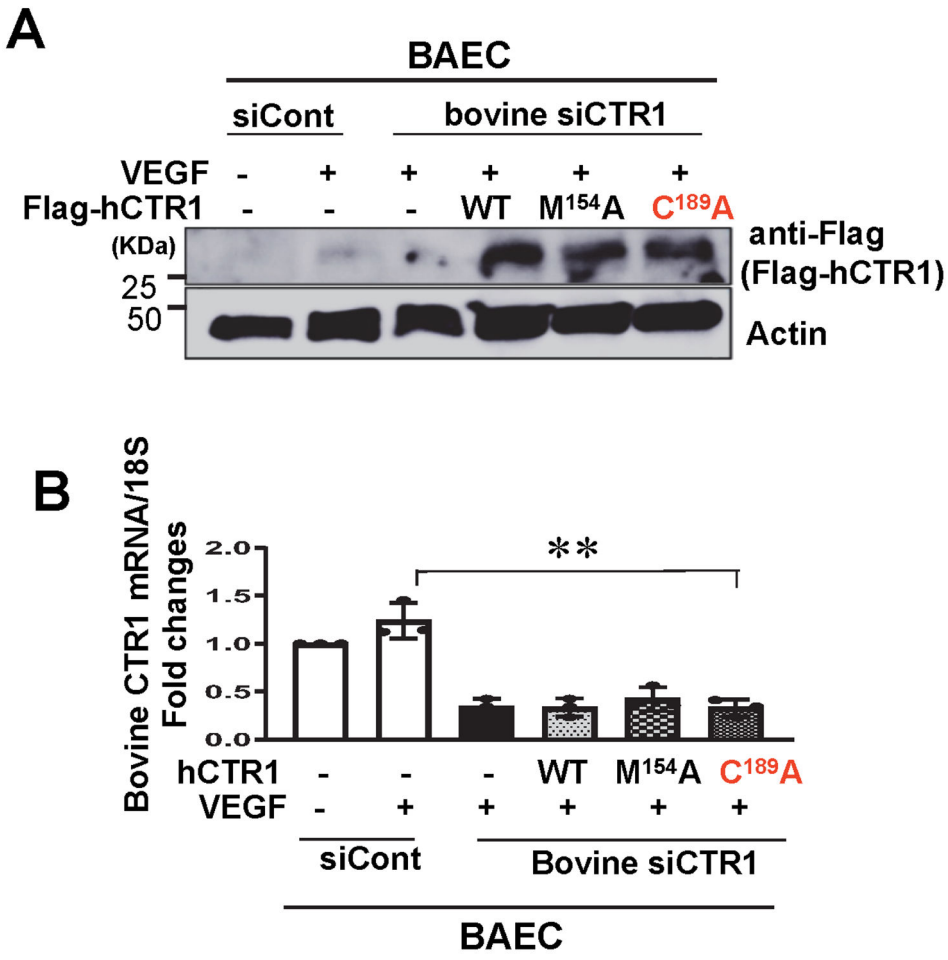

Extended Data Fig. 7. Ectopic expression of Flag-hCTR1-WT, Flag-hCTR1-C189A, or Flag-hCTR1-M^{154}A in bovine aortic endothelial cells (BAECs) transfected with bovine siCont or siCTR1.

Lysates from Fig. 4B were used for IB with anti-Flag antibody to verify ectopic hCTR1 expression or Tubulin antibody (loading control)(**A**). RNA samples were used for real time qPCR analysis to measure bovine CTR1 mRNA (**B**). These data suggest successful knockdown of bovine CTR1 in BAEC with expression of various human CTR1 constructs. (n=3 biologically independent experiments) two-tailed unpaired t-test. **p<0.01. Data are mean ± SEM. Source numerical data and unprocessed blots are available in source data.

Author Manuscript Author Manuscript Author Manuscript Author Manuscript

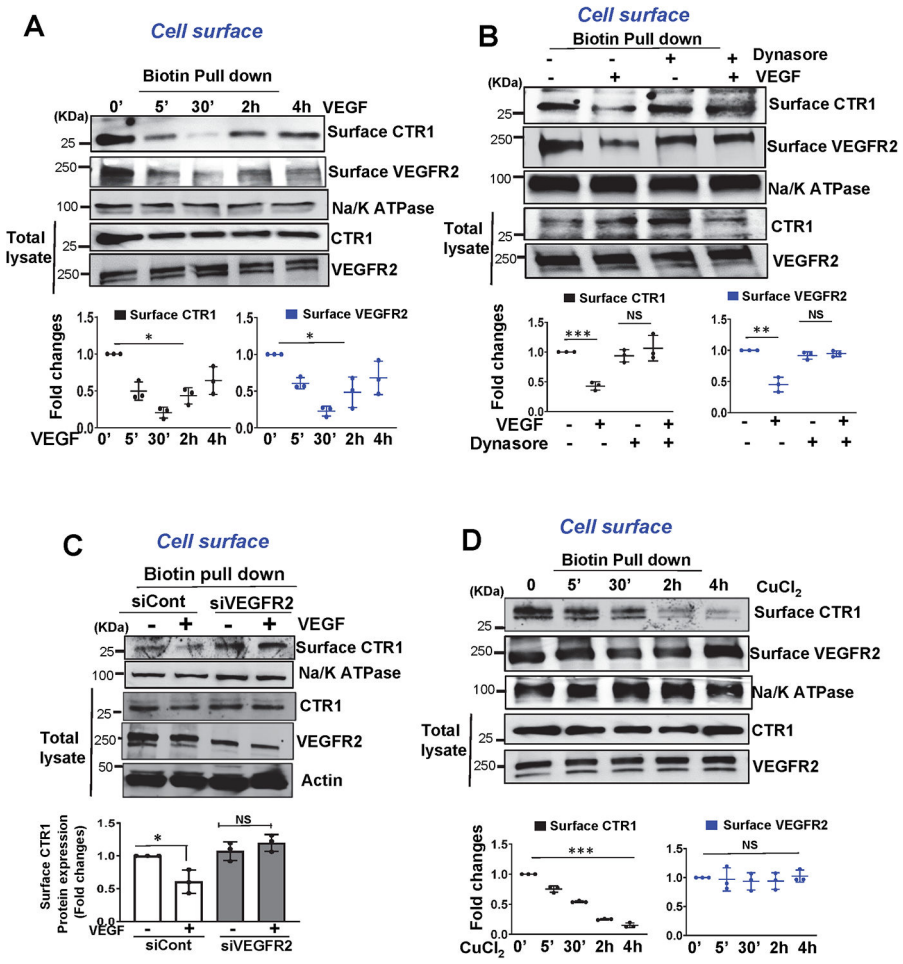

Extended Data Fig. 8. VEGF promotes internalization of CTR1 and VEGFR2 from cell surface in a dynamin- and VEGFR2-dependent manner but $CuCl_2$ promotes CTR1 internalization not VEGFR2.

A, B, C. HUVECs stimulated with VEGF (20ng/ml) for indicated times **(A)** or incubated with dynasore, a dynamin-associated endocytic inhibitor (200nM) (**B**) or transfected with control or VEGFR2 siRNAs were stimulated with VEGF (20 ng/ml) for 30 min (**C**). Cells were labeled with cell surface biotinylation reagent, 1 mM EZ-Link Sulfo-NHS-LC-Biotin, followed by wash and then lysates were pulled down with streptavidin beads, followed by IB with antibodies indicated to detect cell surface CTR1 or VEGFR2 or Na,K-ATPase (cell surface marker). **D.** HUVECs stimulated with $CuCl_2$ (25μM) for indicated times were labeled with cell surface biotinylation reagent, 1 mM EZ-Link Sulfo-NHS-LC-Biotin. After wash, lysates were pulled down with streptavidin beads, followed by IB with antibodies indicated to detect cell surface CTR1 or VEGFR2 or Na,K-ATPase. Bottom panels represent the averaged cell surface CTR1 and VEGFR2 levels expressed as fold changes from the basal control. (n=3 biologically independent experiments). **A, B and D** two-tailed unpaired t-test. **C,** one-way ANOVA followed by Tukey's multiple comparisons analysis, *p<0.05, **p<0.01, ***p<0.001. NS=not significant. Data are mean ± SEM). Source numerical data and unprocessed blots are available in source data.

Author Manuscript
Author Manuscript
Author Manuscript
Author Manuscript

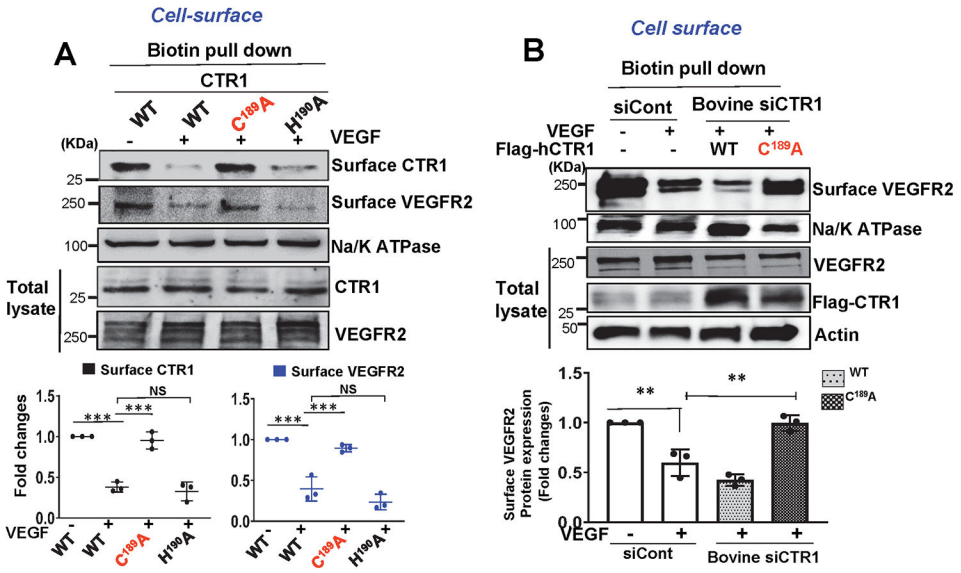

Extended Data Fig. 9. CTR1 sulfenylation at Cys^{189} is required for VEGF-induced internalization of CTR1 and VEGFR2.

A. HUVECs were transfected with Flag-hCTR1-WT or Flag-hCTR1-C^{189}A or Flag-hCTR1-H^{190}A, cells stimulated with VEGF (20ng/ml) for 30min were used for measurement of cell surface CTR1 or VEGFR2 or Na/K ATPase using cell surface biotinylation assay, as in Extended data Fig. 9. **B**. BAECs transfected with bovine sibovine siCTR1 or siControl, together with either Flag-hCTR1-WT, or Flag-hCTR1-C^{189}A were stimulated with VEGF (20ng/ml) for 30 mins. Cells were used to measure cell surface VEGFR2 or Na,K-ATPase protenin expression using cell surface biotinylation assay, as described.) (n=3 biologically independent experiments). one-way ANOVA followed by Tukey's multiple comparisons analysis, *p<0.05, **p<0.01, ***p<0.001. NS=not significant. Data are mean ± SEM. Source numerical data and unprocessed blots are available in source data.

Author Manuscript Author Manuscript Author Manuscript Author Manuscript

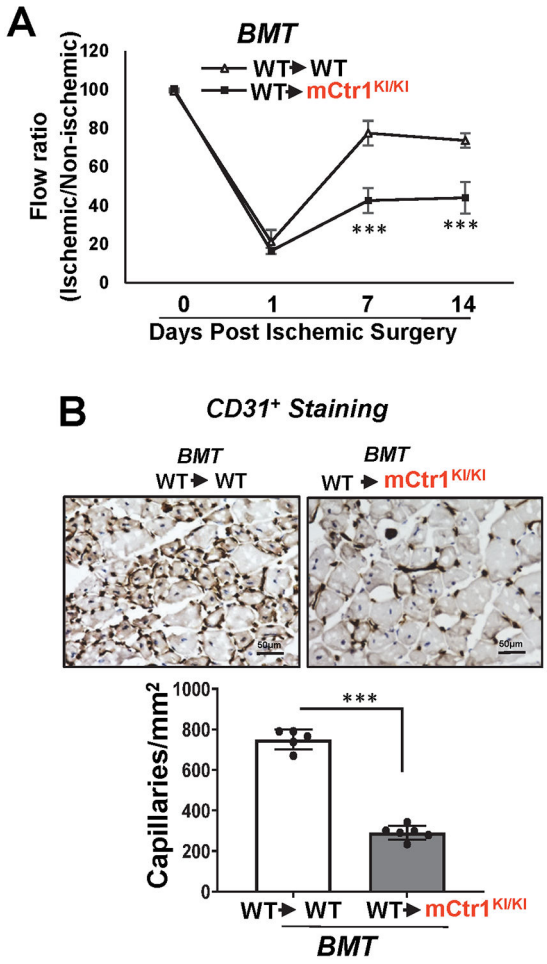

Extended Data Fig. 10. CTR1 sulfenylation in tissue resident cells is required for ischemia-induced angiogenesis in vivo.

A and **B**. Irradiated WT or mCTR1$^{KI/KI}$ mice were transplanted with BM from WT mice. After 6 weeks of BMT, mice were subjected to hindlimb ischemia and limb blood flow using a laser Doppler flow analyzer (**A**). CD31^{+} capillary density in ischemic gastrocnemius muscle at day 14 after ischemic injury were measured (**B**). (n=6 mice per group, representative of two independent experiments, compared with two-way ANOVA followed by Bonferroni's multiple comparison analysis (**A**) or two-tailed unpaired t-test (**B**), ***p<0.001. Data are mean ± SEM). Source numerical data are available in source data.

Supplementary Material

Refer to Web version on PubMed Central for supplementary material.

Acknowledgements

This work was supported by National Institute of Health grants: R01HL135584 (to M.U.-F.), R01HL147550 (to M.U.-F., T.F), R01HL133613 (to T.F., M.U.-F.), R01HL116976 (to T.F., M.U.-F.), R01HL070187 (to T.F.), R35GM135179 (to L.B.P.), R01EY011766, R01EY030500, R21EY032265 (R.B.C.), 1K99EY029373-01A1 to (A.Y.F.); American Heart Association (AHA) Grant 17POST33660754 (to D.A.); Veterans Administration Merit Review Award 2I01BX001232 (to T.F.), 101BX001233 (R.B.C.), The VA Career Scientist Award (IK6BX005228)

Author Manuscript Author Manuscript Author Manuscript Author Manuscript

(to R.B.C.). R.B. Caldwell is the recipient of a Research Career Scientist Award from the Department of Veterans Affairs. The contents do not represent the views of the Department of Veterans Affairs or the United States Government. The funders had no role in study design, data collection and analysis, decision to publish, or preparation of the manuscript. We would like to acknowledge Xuexiu Fang for assisting mouse genotyping in our initial study, and core facilities of the Genome research Division within the Research Resource Center at the University of Illinois at Chicago for DNA sequencing and the Transgenic Mouse and Embryonic Stem Cell Facility at the University of Chicago for embryo injections.

References

1. Simons M, Gordon E & Claesson-Welsh L Mechanisms and regulation of endothelial VEGF receptor signalling. Nat Rev Mol Cell Biol 17, 611–625 (2016). [PubMed: 27461391]
2. Simons M An inside view: VEGF receptor trafficking and signaling. Physiology (Bethesda) 27, 213–222 (2012). [PubMed: 22875452]
3. Eichmann A & Simons M VEGF signaling inside vascular endothelial cells and beyond. Curr Opin Cell Biol 24, 188–193 (2012). [PubMed: 22366328]
4. Lanahan A et al. The neuropilin 1 cytoplasmic domain is required for VEGF-A-dependent arteriogenesis. Dev Cell 25, 156–168 (2013). [PubMed: 23639442]
5. Sawamiphak S et al. Ephrin-B2 regulates VEGFR2 function in developmental and tumour angiogenesis. Nature 465, 487–491 (2010). [PubMed: 20445540]
6. Genet G et al. Endophilin-A2 dependent VEGFR2 endocytosis promotes sprouting angiogenesis. Nat Commun 10, 2350 (2019). [PubMed: 31138815]
7. Tang X et al. Endothelium-specific deletion of Nox4 delays retinal vascular development and mitigates pathological angiogenesis. Angiogenesis (2020).
8. Craige SM et al. NADPH oxidase 4 promotes endothelial angiogenesis through endothelial nitric oxide synthase activation. Circulation 124, 731–740 (2011). [PubMed: 21788590]
9. Evangelista AM, Thompson MD, Bolotina VM, Tong X & Cohen RA Nox4- and Nox2-dependent oxidant production is required for VEGF-induced SERCA cysteine-674 S-glutathiolation and endothelial cell migration. Free Radic Biol Med 53, 2327–2334 (2012). [PubMed: 23089226]
10. Kim YM et al. ROS-induced ROS release orchestrated by Nox4, Nox2, and mitochondria in VEGF signaling and angiogenesis. Am J Physiol Cell Physiol 312, C749–C764 (2017). [PubMed: 28424170]
11. Schroder K et al. Nox4 is a protective reactive oxygen species generating vascular NADPH oxidase. Circ Res 110, 1217–1225 (2012). [PubMed: 22456182]
12. Tojo T et al. Role of gp91phox (Nox2)-containing NAD(P)H oxidase in angiogenesis in response to hindlimb ischemia. Circulation 111, 2347–2355 (2005). [PubMed: 15867174]
13. Urao N et al. Critical role of endothelial hydrogen peroxide in post-ischemic neovascularization. PLoS One 8, e57618 (2013). [PubMed: 23472092]
14. Ushio-Fukai M Redox signaling in angiogenesis: role of NADPH oxidase. Cardiovasc Res 71, 226–235 (2006). [PubMed: 16781692]
15. Ushio-Fukai M VEGF signaling through NADPH oxidase-derived ROS. Antioxid Redox Signal 9, 731–739 (2007). [PubMed: 17511588]
16. Ushio-Fukai M & Urao N Novel role of NADPH oxidase in angiogenesis and stem/progenitor cell function. Antioxid Redox Signal 11, 2517–2533 (2009). [PubMed: 19309262]
17. Charles RL et al. Protein sulfenation as a redox sensor: proteomics studies using a novel biotinylated dimedone analogue. Mol Cell Proteomics 6, 1473–1484 (2007). [PubMed: 17569890]
18. Poole LB, Karplus PA & Claiborne A Protein sulfenic acids in redox signaling. Annu Rev Pharmacol Toxicol 44, 325–347 (2004). [PubMed: 14744249]
19. Poole LB & Nelson KJ Discovering mechanisms of signaling-mediated cysteine oxidation. Curr Opin Chem Biol 12, 18–24 (2008). [PubMed: 18282483]
20. Fukai T, Ushio-Fukai M & Kaplan JH Copper transporters and copper chaperones: roles in cardiovascular physiology and disease. Am J Physiol Cell Physiol 315, C186–C201 (2018). [PubMed: 29874110]

Author Manuscript Author Manuscript Author Manuscript Author Manuscript

21. Narayanan G, R BS, Vuyyuru H, Muthuvel B & Konerirajapuram Natrajan S CTR1 silencing inhibits angiogenesis by limiting copper entry into endothelial cells. PLoS One 8, e71982 (2013). [PubMed: 24039729]
22. Harris ED A requirement for copper in angiogenesis. Nutr Rev 62, 60–64 (2004). [PubMed: 15080367]
23. Brewer GJ Tetrathiomolybdate anticopper therapy for Wilson's disease inhibits angiogenesis, fibrosis and inflammation. J Cell Mol Med 7, 11–20 (2003). [PubMed: 12767257]
24. Kaplan JH & Maryon EB How Mammalian Cells Acquire Copper: An Essential but Potentially Toxic Metal. Biophys J 110, 7–13 (2016). [PubMed: 26745404]
25. Maryon EB, Molloy SA, Ivy K, Yu H & Kaplan JH Rate and regulation of copper transport by human copper transporter 1 (hCTR1). The Journal of biological chemistry 288, 18035–18046 (2013). [PubMed: 23658018]
26. Eisses JF & Kaplan JH The mechanism of copper uptake mediated by human CTR1: a mutational analysis. The Journal of biological chemistry 280, 37159–37168 (2005). [PubMed: 16135512]
27. Puig S, Lee J, Lau M & Thiele DJ Biochemical and genetic analyses of yeast and human high affinity copper transporters suggest a conserved mechanism for copper uptake. The Journal of biological chemistry 277, 26021–26030 (2002). [PubMed: 11983704]
28. Clifford RJ, Maryon EB & Kaplan JH Dynamic internalization and recycling of a metal ion transporter: Cu homeostasis and CTR1, the human Cu(+) uptake system. J Cell Sci 129, 1711–1721 (2016). [PubMed: 26945057]
29. Molloy SA & Kaplan JH Copper-dependent recycling of hCTR1, the human high affinity copper transporter. The Journal of biological chemistry 284, 29704–29713 (2009). [PubMed: 19740744]
30. Brady DC et al. Copper is required for oncogenic BRAF signalling and tumorigenesis. Nature 509, 492–496 (2014). [PubMed: 24717435]
31. Tsai CY, Finley JC, Ali SS, Patel HH & Howell SB Copper influx transporter 1 is required for FGF, PDGF and EGF-induced MAPK signaling. Biochem Pharmacol 84, 1007–1013 (2012). [PubMed: 22842628]
32. Turski ML et al. A novel role for copper in Ras/mitogen-activated protein kinase signaling. Molecular and cellular biology 32, 1284–1295 (2012). [PubMed: 22290441]
33. Chen GF et al. Copper Transport Protein Antioxidant-1 Promotes Inflammatory Neovascularization via Chaperone and Transcription Factor Function. Sci Rep 5, 14780 (2015). [PubMed: 26437801]
34. Gariano RF & Gardner TW Retinal angiogenesis in development and disease. Nature 438, 960–966 (2005). [PubMed: 16355161]
35. Liu Z et al. Glycolysis links reciprocal activation of myeloid cells and endothelial cells in the retinal angiogenic niche. Sci Transl Med 12 (2020).
36. Wang Y et al. Ephrin-B2 controls VEGF-induced angiogenesis and lymphangiogenesis. Nature 465, 483–486 (2010). [PubMed: 20445537]
37. Das A et al. Endothelial Antioxidant-1: a Key Mediator of Copper-dependent Wound Healing in vivo. Sci Rep 6, 33783 (2016). [PubMed: 27666810]
38. Kuo YM, Zhou B, Cosco D & Gitschier J The copper transporter CTR1 provides an essential function in mammalian embryonic development. Proc Natl Acad Sci U S A 98, 6836–6841 (2001). [PubMed: 11391004]
39. Lee J, Prohaska JR & Thiele DJ Essential role for mammalian copper transporter Ctr1 in copper homeostasis and embryonic development. Proc Natl Acad Sci U S A 98, 6842–6847 (2001). [PubMed: 11391005]
40. Kim YM et al. Redox Regulation of Mitochondrial Fission Protein Drp1 by Protein Disulfide Isomerase Limits Endothelial Senescence. Cell Rep 23, 3565–3578 (2018). [PubMed: 29924999]
41. Shanbhag V et al. ATP7A delivers copper to the lysyl oxidase family of enzymes and promotes tumorigenesis and metastasis. Proc Natl Acad Sci U S A 116, 6836–6841 (2019). [PubMed: 30890638]
42. Baker AM et al. Lysyl oxidase plays a critical role in endothelial cell stimulation to drive tumor angiogenesis. Cancer Res 73, 583–594 (2013). [PubMed: 23188504]

Author Manuscript Author Manuscript Author Manuscript Author Manuscript

43. Ash D et al. The P-type ATPase transporter ATP7A promotes angiogenesis by limiting autophagic degradation of VEGFR2. Nat Commun 12, 3091 (2021). [PubMed: 34035268]
44. Nelson KJ et al. Use of dimedone-based chemical probes for sulfenic acid detection methods to visualize and identify labeled proteins. Methods Enzymol 473, 95–115 (2010). [PubMed: 20513473]
45. Okur MN, Russo A & O'Bryan JP Receptor tyrosine kinase ubiquitylation involves the dynamic regulation of Cbl-Spry2 by intersectin 1 and the Shp2 tyrosine phosphatase. Molecular and cellular biology 34, 271–279 (2014). [PubMed: 24216759]
46. Kang DH et al. Peroxiredoxin II is an essential antioxidant enzyme that prevents the oxidative inactivation of VEGF receptor-2 in vascular endothelial cells. Mol Cell 44, 545–558 (2011). [PubMed: 22099303]
47. Lee J, Petris MJ & Thiele DJ Characterization of mouse embryonic cells deficient in the ctr1 high affinity copper transporter. Identification of a Ctr1-independent copper transport system. The Journal of biological chemistry 277, 40253–40259 (2002). [PubMed: 12177073]
48. Rezende F et al. Knock out of the NADPH oxidase Nox4 has no impact on life span in mice. Redox Biol 11, 312–314 (2017). [PubMed: 28038425]
49. Ashino T et al. Unexpected role of the copper transporter ATP7A in PDGF-induced vascular smooth muscle cell migration. Circ Res 107, 787–799 (2010). [PubMed: 20671235]
50. Ikeda S et al. Novel role of ARF6 in vascular endothelial growth factor-induced signaling and angiogenesis. Circ Res 96, 467–475 (2005). [PubMed: 15692085]
51. van Lessen M et al. Regulation of vascular endothelial growth factor receptor function in angiogenesis by numb and numb-like. Arterioscler Thromb Vasc Biol 35, 1815–1825 (2015). [PubMed: 26069237]
52. Pan Q et al. Blocking neuropilin-1 function has an additive effect with anti-VEGF to inhibit tumor growth. Cancer Cell 11, 53–67 (2007). [PubMed: 17222790]
53. Tsai CY, Larson CA, Safaei R & Howell SB Molecular modulation of the copper and cisplatin transport function of CTR1 and its interaction with IRS-4. Biochem Pharmacol 90, 379–387 (2014). [PubMed: 24967972]
54. Lee S, Howell SB & Opella SJ NMR and mutagenesis of human copper transporter 1 (hCtr1) show that Cys-189 is required for correct folding and dimerization. Biochim Biophys Acta 1768, 3127–3134 (2007). [PubMed: 17959139]
55. Ran FA et al. Genome engineering using the CRISPR-Cas9 system. Nat Protoc 8, 2281–2308 (2013). [PubMed: 24157548]
56. Clement K et al. CRISPResso2 provides accurate and rapid genome editing sequence analysis. Nat Biotechnol 37, 224–226 (2019). [PubMed: 30809026]
57. Zhou HJ et al. SUMOylation of VEGFR2 regulates its intracellular trafficking and pathological angiogenesis. Nat Commun 9, 3303 (2018). [PubMed: 30120232]
58. Pitulescu ME, Schmidt I, Benedito R & Adams RH Inducible gene targeting in the neonatal vasculature and analysis of retinal angiogenesis in mice. Nat Protoc 5, 1518–1534 (2010). [PubMed: 20725067]
59. Lee M, Choy WC & Abid MR Direct sensing of endothelial oxidants by vascular endothelial growth factor receptor-2 and c-Src. PLoS One 6, e28454 (2011). [PubMed: 22145046]
60. Oshikawa J et al. Novel role of p66Shc in ROS-dependent VEGF signaling and angiogenesis in endothelial cells. Am J Physiol Heart Circ Physiol 302, H724–732 (2012). [PubMed: 22101521]
61. Oshikawa J et al. Extracellular SOD-derived H2O2 promotes VEGF signaling in caveolae/lipid rafts and post-ischemic angiogenesis in mice. PLoS One 5, e10189 (2010). [PubMed: 20422004]
62. Pasula S et al. Endothelial epsin deficiency decreases tumor growth by enhancing VEGF signaling. J Clin Invest 122, 4424–4438 (2012). [PubMed: 23187125]

Author Manuscript Author Manuscript Author Manuscript Author Manuscript

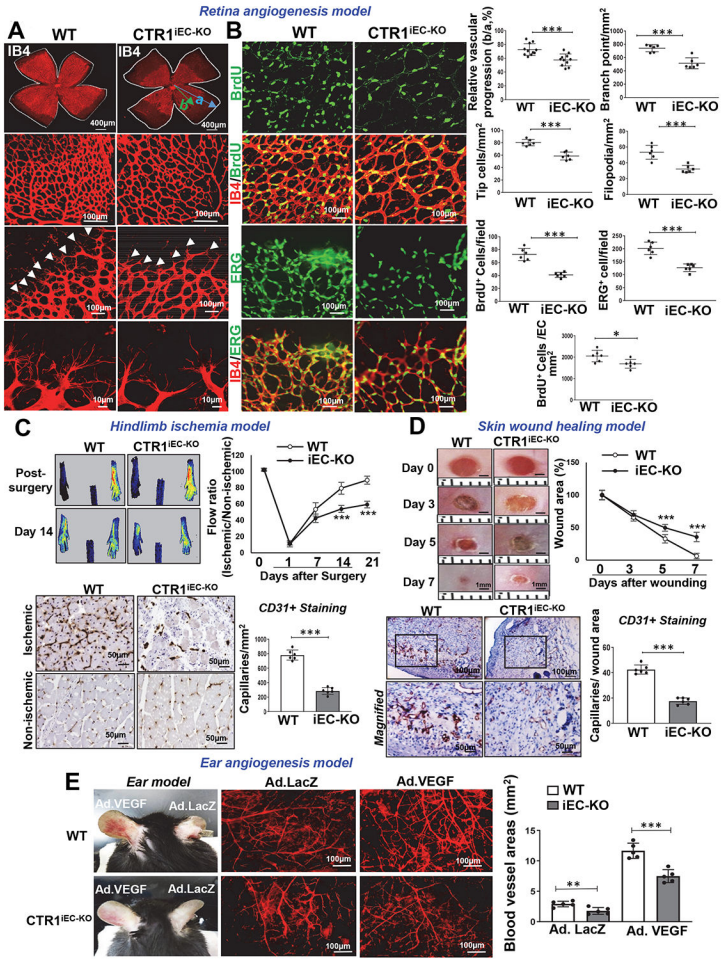

Figure 1: Endothelial CTR1 is required for postnatal angiogenesis *in vivo*.

A and B. Retinal whole-mount staining with Isolectin B4 (IB4) of P6 WT and CTR1^{iECKO} mice. Arrowheads show tip cell sprouting and filopodia (**A**). BrdU or ERG (endothelial nuclei marker)(green) co-stained with or without IB4 (red) in P6 retinal flatmounts of WT and CTR1^{iECKO} mice (**B**). Right panels show quantification of vascular progression length, numbers of branch point, tip cells and filopodia (**A**) and BrdU -or ERG-positive cells or endothelial BrdU-positive cells in the field (**B**), (vascular progression: n=11 samples each for WT and CTR1^{iECKO}; branch point, tip cells, filopodia, BrdU+, ERG+: n=6 samples each for WT and CTR1^{iECKO} respectively, compared with two-tailed unpaired t-test). **C.** Blood flow recovery after hindlimb ischemia as determined by the ratio of foot perfusion between ischemic (left) and non-ischemic (right) legs in WT and CTR1^{iECKO} mice (right), two-way ANOVA followed by Bonferroni's multiple comparison analysis. Left panels show representative laser Doppler images of legs at day 14. Bottom panels show CD31^{+} staining (capillary density) in ischemic and nonischemic gastrocnemius muscles at day 14. Right panel shows quantification, (n=6 mice per group, representative of two independent experiments, compared with two-tailed unpaired t-test). **D.** Excisional cutaneous wounds were created using a 3 mm biopsy punch on the dorsal skin of WT and CTR1^{iECKO} mice. Ruler notches=1 mm. Right panel shows the quantification of wound closure rates,

Author Manuscript Author Manuscript Author Manuscript Author Manuscript

two-way ANOVA followed by Bonferroni's multiple comparison analysis. Bottom images show CD31 staining of wounded tissues at day 7 with magnified images in Box. Right panel shows quantification, (n=6 mice per group, representative of two independent experiments, compared with two-tailed unpaired t-test). **E.** Adenovirus encoding VEGF164 (1×10^9 pfu) (Ad-VEGF) or β-galactosidase (Ad-LacZ) was intradermally injected into the right and left ear skin of WT and $CTR1^{iECKO}$ mice, respectively. Ear vasculature (red) was visualized by a whole-mount staining with CD31. Right panel shows the quantification of vessel density. (n=5 mice per group, representative of two independent experiments, two-tailed unpaired t-test. *p<0.05, **p<0.005, ***p<0.001. Data are mean ± SEM). Source numerical data are available in source data.

Author Manuscript Author Manuscript Author Manuscript Author Manuscript

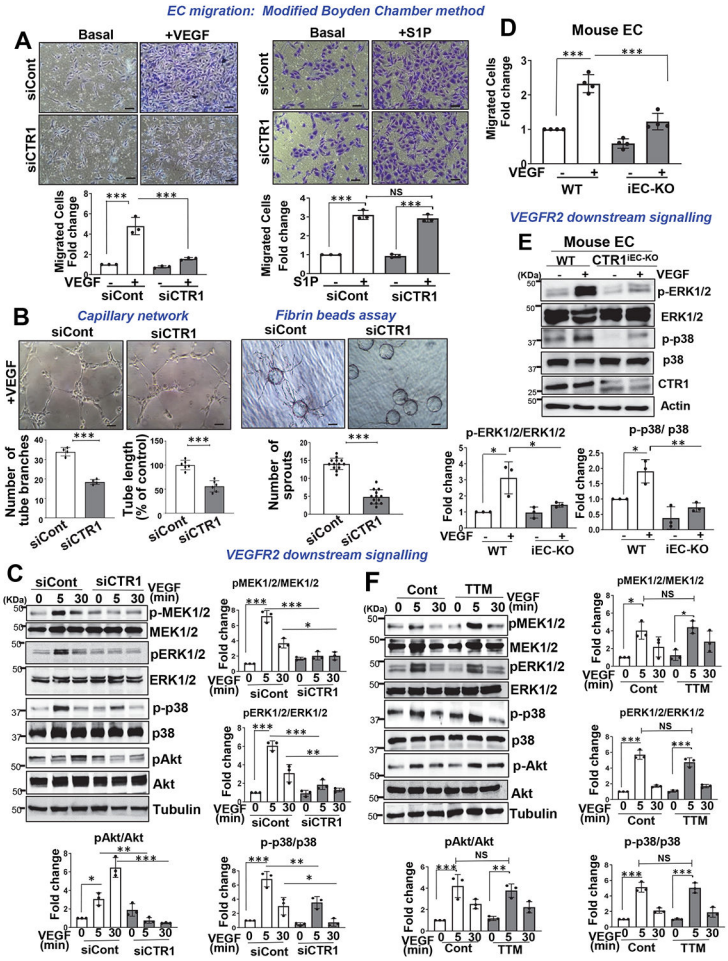

Figure 2: CTR1 knockdown inhibits VEGF-induced signaling and angiogenesis in ECs.

A and D. EC migration measured by the modified Boyden chamber method in HUVECs transfected with control or CTR siRNAs stimulated with VEGF (20ng/ml) or S1P (10μM) for 6 h (**A**) or ECs isolated from WT (WT ECs) or Ctr1^{iECKO} mice stimulated with VEGF for 8h (**D**). Graph represents the averaged fold change of migrated cells over the basal control (n=3 biologically independent experiments, one-way ANOVA followed by Bonferroni's multiple comparison analysis). Scale bars=50μm. **B.** Capillary-like network formation on Matrigel analyzed by the number of tube branches or capillary tube length (left). Capillary sprouting formation in the fibrin clot analyzed by the number of sprouts (right). (n=3 biologically independent experiments, two-tailed unpaired t-test). Scale bars=50μm. **C,E,F**. HUVECs transfected with control or CTR1 siRNAs (**C**); or WT ECs or Ctr1^{iECKO} ECs (**E**); HUVECs treated with the Cu chelator TTM (20 nM) for 24h (**F**) stimulated with VEGF (20ng/ml) were used to measure VEGF signaling using Western blotting. Graphs represent the averaged fold change of phosphorylated proteins/total proteins over the basal control (n=3 biologically independent experiments). **C,** one-way ANOVA followed by Tukey's multiple comparisons analysis. **E,** two-tailed unpaired t-test. **F,** one-way ANOVA followed by Bonferroni's multiple comparison analysis. *p<0.05, **p<0.01,

Author Manuscript Author Manuscript Author Manuscript Author Manuscript

***p<0.001. Data are mean ± SEM. Source numerical data and unprocessed blots are available in source data.

Author Manuscript Author Manuscript Author Manuscript Author Manuscript

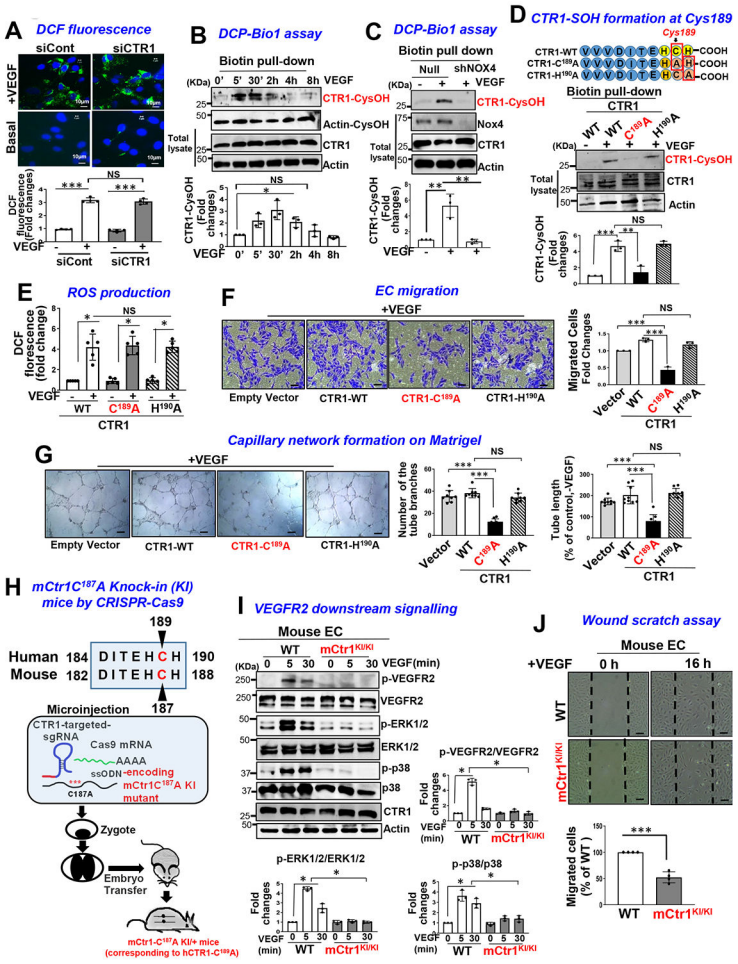

Figure 3: VEGF induces CTR1-Cys^{189}OH formation, which promotes angiogenesis in ECs.

A. HUVECs transfected with control or CTR1 siRNAs stimulated with VEGF (20 ng/ml) for 5 min were used for dichlorofluorescein (DCF) fluorescence and DAPI staining (blue). Bottom panel represents the averaged fold change from the basal control (n=3 biologically independent experiments, one-way ANOVA followed by Bonferroni's multiple comparison analysis). **B, C, D.** HUVECs stimulated with VEGF for indicated time (**B**), or HUVECs infected with Ad.null or Ad.shNox4 (**C**), or transfected with Flag-hCTR1-WT, Flag-hCTR1-C^{189}A or Flag-hCTR1-H^{190}A (**D**) stimulated with VEGF for 5 min were used for DCP-Bio1 assay. In D, top panel: Amino acid sequence of the human CTR1 C terminus in WT and two mutants (CTR1-WT, CTR1-C^{189}A, CTR1-H^{190}A). DCP-Bio1-labeled lysates pulled down with streptavidin beads were immunoblotted (IB) with anti-CTR1 or actin (**B**) or anti-CTR1 (**C**) or Flag (**D**) to measure CTR1-CysOH formation. (n=3 biologically independent experiments, two-tailed unpaired t-test). *p =0.0143, ** P=0.0072, **P=0.0063, ***P=0.0006, **P=0.005. **E, F, G**. HUVECs transfected with empty vector, Flag-CTR1-WT, Flag-CTR1-C^{189}A or Flag-CTR1-H^{190}A were used to measure DCF fluorescence stimulated with VEGF for 5 min (**E**), or EC migration (Boyden chamber assay) stimulated with VEGF for 6 h (**F**), or capillary network formation on Matrigel stimulated with VEGF for 4 h. Scale bars=50μm. **G**. Bar graphs represent the averaged fold change from the basal

Author Manuscript Author Manuscript Author Manuscript Author Manuscript

control. **H.** Schematic diagram of CRISPR-generated “redox dead” mCtr1-C^{187}A (human CTR1-C^{189}A) knock-in (KI)($mCtr1^{KI/+}$ mice. CRISPR sgRNA targeting the mCtr1 gene, Cas9 mRNA, and single stranded oligo donor DNA (ssODN) encoding CTR1 mutations was injected into mouse zygotes. **I and J.** Aortic ECs from WT and $mCtr1^{KI/KI}$ mice were used to measure VEGF signaling using Western blots (**I)** or EC migration using a wound scratch assay. Scale bars=50μm. **J**. Graph represents the averaged % of migrated cells at wounded area compared to WT ECs. **E, F, G, I and J.** (n=3 biologically independent cells, two-tailed unpaired t-test). *p<0.05, **p<0.01, ***p<0.001. NS=not significant. Data are mean ± SEM. Source numerical data and unprocessed blots are available in source data.

Author Manuscript Author Manuscript Author Manuscript Author Manuscript

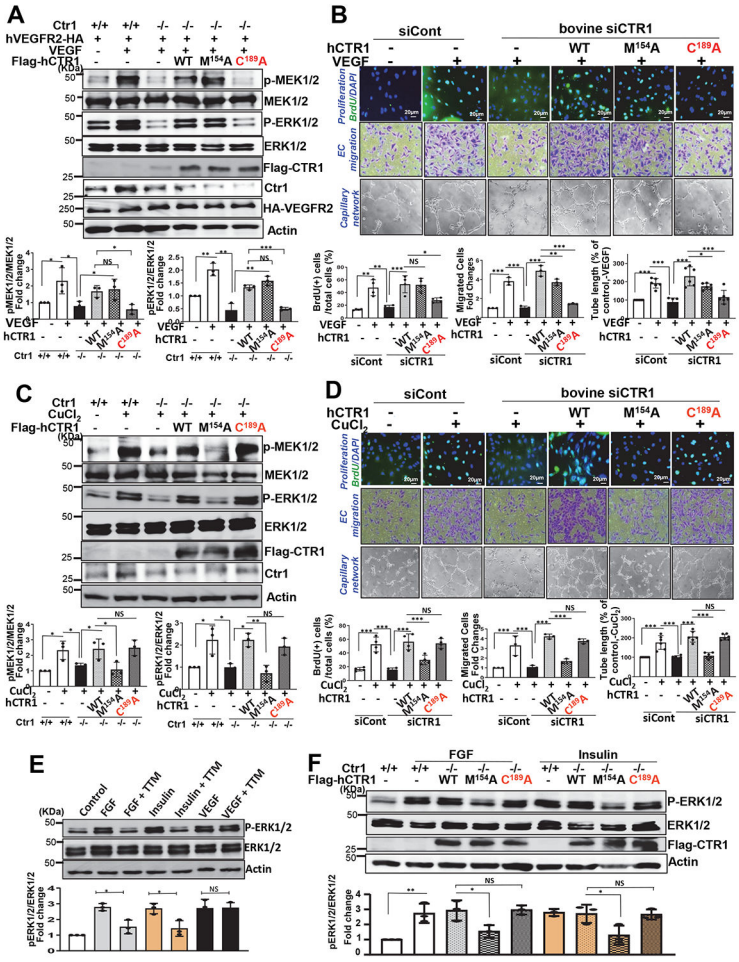

Figure 4: Role of CTR1-Cys^{189}OH formation and Cu transport function in VEGF-, Cu-, and other growth factor-induced signaling and angiogenic responses.

A and C. Ctr1$^{-/-}$ MEFs transfected with HA-hVEGFR2 (A only), Flag-hCTR1-WT, Flag-hCTR1-C^{189}A or Flag-hCTR1-M^{154}A; or Ctr$^{+/+}$ MFFs transfected with HA-hVEGFR2 (A only) or empty vector were stimulated with VEGF (20ng/ml**)(A)** or $CuCl_2$ (100μM)(**C**), followed by Western blotting. **B and D.** Bovine aortic endothelial cells (BAECs) were transfected with siControl or siCTR1, and siCTR1-treated ECs were also transfected with empty vector, Flag-hCTR1-WT, Flag-hCTR1-C^{189}A, or Flag-hCTR1-M^{154}A. These cells were used to measure VEGF (20ng/ml)(**B**)- or $CuCl_2$ (100μM)(**D**)-induced cell proliferation (BrdU incorporation), cell migration (modified Boyden chamber assay) or capillary network formation on Matrigel. **E and F.** HUVECs treated with Cu chelator, TTM (20nM) for 24h (**E**), CTR1$^{+/+}$ or Ctr1$^{-/-}$ MEFs transfected with Flag-hCTR1-WT, Flag-hCTR1-C^{189}A or Flag-hCTR1-M^{154}A **(F**) were stimulated with FGF (1ng/ml) or insulin (25μg/ml) for 10 min. Lysates were used to measure p-ERK1/2, and their total proteins using Western blots. Graphs represent the averaged fold change of phosphorylated proteins/total proteins over the basal control (n=3 biologically independent experiments). **A and C**, two-tailed unpaired t-test. **B, D, E and F,** one-way ANOVA followed by Tukey's multiple comparisons analysis. *p<0.05, **p<0.01, ***p<0.001. NS=not significant. Data are mean ± SEM. Source numerical data and unprocessed blots are available in source data.

Author Manuscript Author Manuscript Author Manuscript Author Manuscript

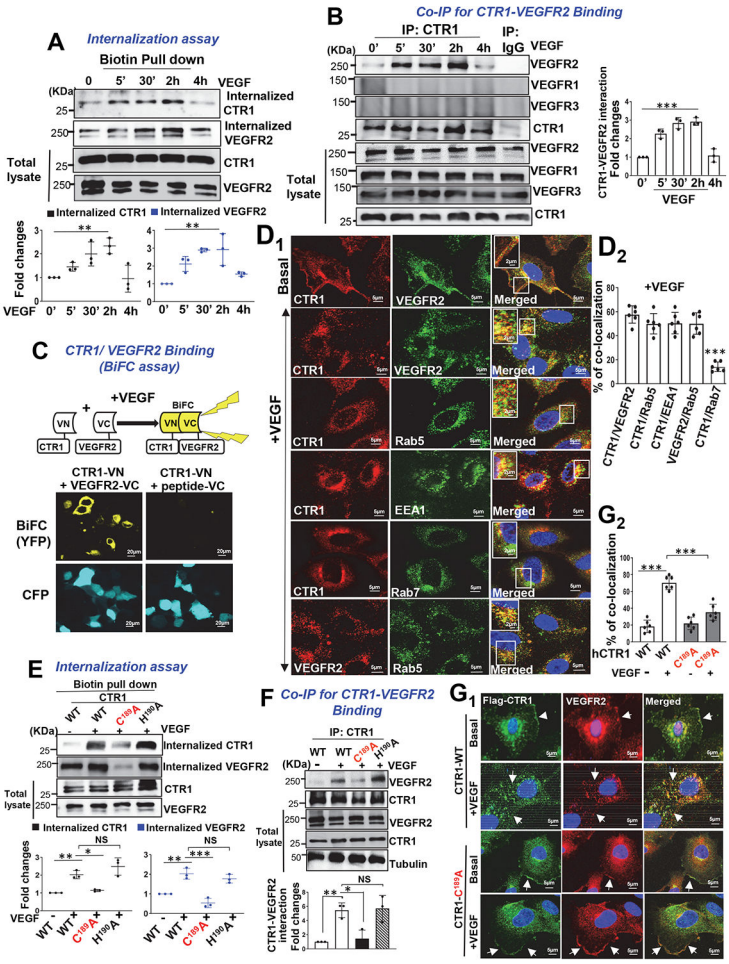

Figure 5: CTR1-Cys^{189}OH formation is required for VEGF-induced CTR1 binding to VEGFR2 and their co-internalization to early endosomes.

A. Cell surface of HUVECs were labeled with 1 mM EZ-Link Sulfo-NHS-SS-Biotin for 60min, followed by VEGF (20ng/ml) stimulation. After wash, lysates were biotin-pulled down, followed by IB with anti-CTR1 or VEGFR2 to measure their internalization. Bottom panels represent averaged fold change over the basal control. **B.** HUVECs stimulated with VEGF (20ng/ml) were immunoprecipitated (IP) with anti-CTR1 or IgG (negative control), followed by IB with antibodies indicated. Right panel represents the averaged fold change of CTR1/VEGFR2 ratio over the basal ratio. **A and B.** (n=3 biologically independent experiments, one-way ANOVA followed by Bonferroni's multiple comparison analysis). **P= 0.0064, **P= 0.0014. **C.** BiFC assay. HEK293 cells co-transfected with Flag-hCTR1-VN173 and HA-hVEGFR2-VC155 or peptide-VC155 (negative control) with ECFP were stimulated with VEGF for 30 min. The YFP (Yellow) shows interaction of CTR1 and VEGFR2. (the experiment is representative of 3 independent experiments that yielded similar results) **D**. HUVECs stimulated with VEGF for 20 min were co-stained for CTR1 with VEGFR2 or early endosome markers (Rab5 or EEA1) or late endosome marker (Rab7). Yellow fluorescence shows their colocalization in the white box in the merged images (**D1**). Right panel shows the averaged % of co-localization (**D2**). **E and F.** HUVECs transfected with Flag-hCTR1-WT, Flag-hCTR1-C^{189}A or Flag-hCTR1-H^{190}A stimulated with VEGF

Author Manuscript Author Manuscript Author Manuscript Author Manuscript

(20ng/ml) for 30 min were used to measure internalized CTR1 (detected by anti-Flag) and VEGFR2 using cell surface biotinylation assay (**E**) or Co-IP for CTR1-VEGFR2 (**F**). (n=3 biologically independent experiments, one-way ANOVA followed by Tukey's multiple comparisons analysis). **p= 0.0071, *p= 0.0159, **p= 0.0017, ***p= 0.0001, **p= 0.0084, *p= 0.0153. **G.** HUVECs transfected with Flag-hCTR1-WT or Flag-hCTR1-$C^{189}A$ stimulated with VEGF for 30min were used for CTR1-VEGFR2 co-localization analysis using anti-Flag (green for CTR1) and anti-VEGFR2 (red) (**G1**). White arrow heads show their colocalization. Upper panel shows the averaged % of co-localization (**G2**). **D2 and G2.** (n=6 images examined over 3 biologically independent experiments; one-way ANOVA followed by Bonferroni's multiple comparison analysis). *p<0.05, **p<0.01, ***p<0.001. NS=not significant. Data are mean ± SEM. Source numerical data and unprocessed blots are available in source data.

Author Manuscript Author Manuscript Author Manuscript Author Manuscript

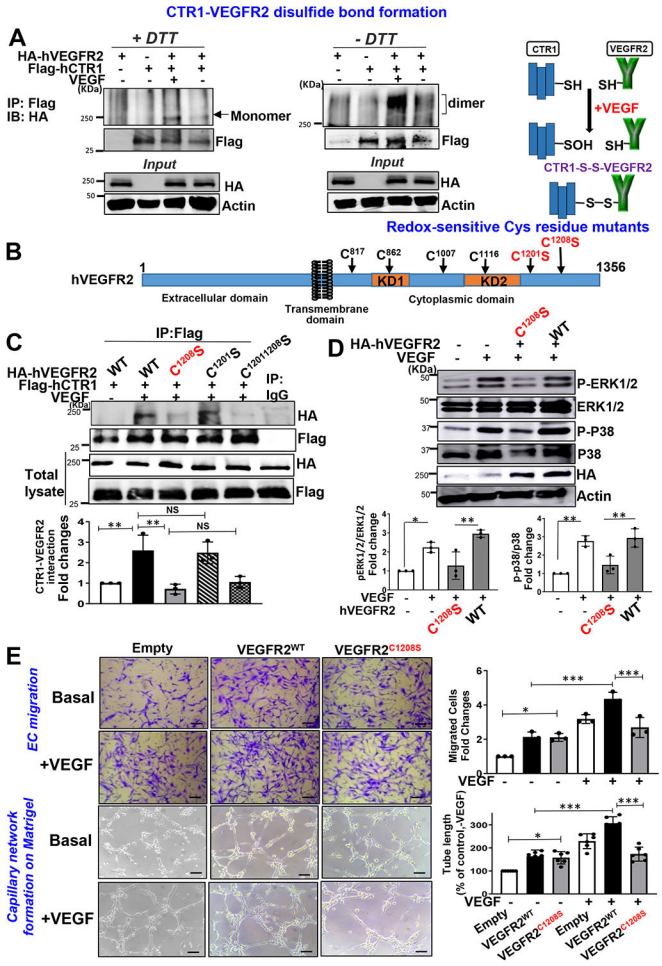

Figure 6: CTR1 Cys^{189}OH forms disulfide bond with VEGFR2 at Cys^{1208}, which promotes VEGFR2 signaling and angiogenic responses.

A. Right panel Schematic diagram of disulfide formation between CTR1-S(Cys^{189})OH and VEGFR2-SH after VEGF stimulation. Left panel, HEK293T cells transfected with HA-hVEGFR2-WT and Flag-hCTR1-WT were stimulated with VEGF (20ng/ml) for 10 min. Lysates were IP with anti-Flag, followed by SDS-PAGE under nonreducing (-DTT) and reducing (+DTT) conditions and IB with anti-HA antibody (the experiment is representative of 3 independent experiments that yielded similar results). **B.** VEGFR2 protein structure. VEGFR2 is composed of an extracellular domain, transmembrane domain, two separate kinase domains (KD1 and KD2), and C-terminal domain. The highly conserved six cysteine residues in VEGFRs are indicated by arrows and redox sensitive cysteine residues (C^{1201} and C^{1208}) are shown in red. **C**. HEK cells co-transfected with Flag-hCTR1 WT and various HA-hVEGFR2 mutants (VEGFR2-WT, C^{1201}S, C^{1208}S, C^{1201}, ^{1208}S) were stimulated with VEGF (20 ng/mL) for 10 min. Lysates were IP with anti-Flag or IgG (negative control), followed by IB with anti-HA antibody. (n=3 biologically independent experiments, one-way ANOVA followed by Tukey's multiple comparisons analysis). **P=0.0093, **P=0.0029. **D and E.** BAECs transfected with empty vector, HA-VEGFR2-WT, or -VEGFR2-C^{1208}S were used to measure VEGFR2 signaling stimulated by VEGF for 5 min using Western blotting (**D**) (n=3 biologically independent experiments, one-way ANOVA followed by

Author Manuscript Author Manuscript Author Manuscript Author Manuscript

Tukey's multiple comparisons analysis). *P=0.021, **P=0.0037, **P=0.0019, **P=0.006. In parallel, cells were used to measure VEGF-induced EC migration using the Boyden chamber assay or capillary network formation on Matrigel (**E**). Scale bars=50μm. Bar graphs represent the averaged fold change from the basal control. (n=3 biologically independent experiments, one-way ANOVA followed by Tukey's multiple comparisons analysis). *p<0.05, **p<0.01, ***p<0.001. NS=not significant. Data are mean ± SEM. Source numerical data and unprocessed blots are available in source data.

Author Manuscript Author Manuscript Author Manuscript Author Manuscript

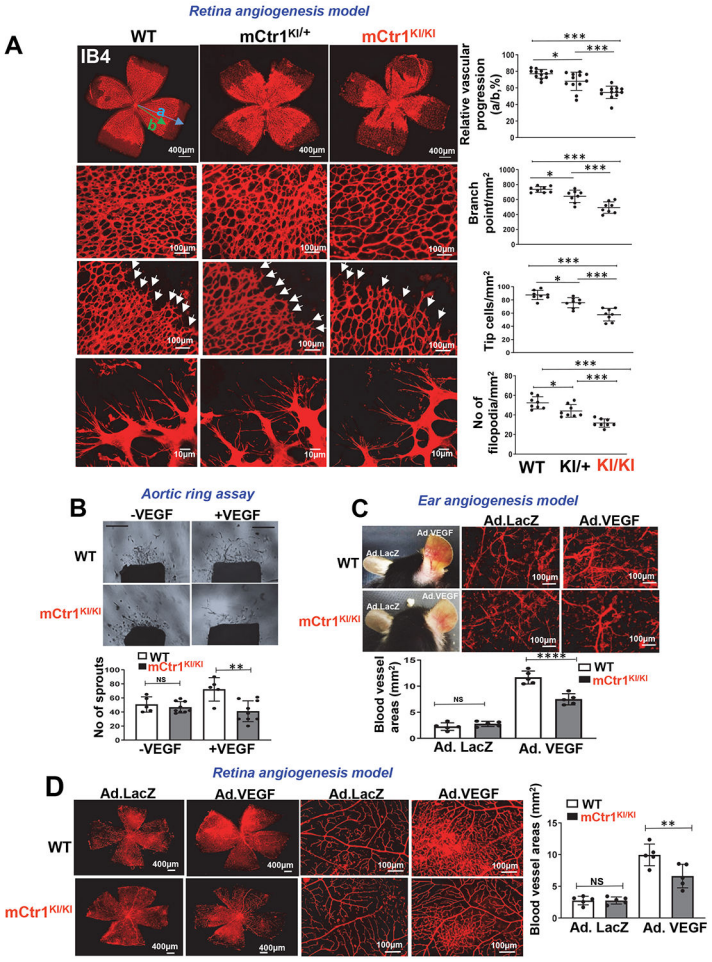

Figure 7: CTR1-CysOH formation is required for developmental and VEGF-induced angiogenesis *in vivo*.

A. Retinal whole-mount staining with Isolectin B4 (IB4) of P5 WT, "redox dead" mCTR1$^{KI/+}$ or mCTR1$^{KI/KI}$ mice. Arrowheads show tip cell sprouting and filopodia. Right panels show quantification of vascular progression length, numbers of branch point, tip cells and filopodia. (vascular progression: n=12 samples each for WT, mCTR1$^{KI/+}$, and mCTR1$^{KI/KI}$; branch point, tip cells, filopodia: n=8 samples each for WT, mCTR1$^{KI/+}$, and mCTR1$^{KI/KI}$ respectively, compared with One-way ANOVA followed by Tukey's multiple comparisons analysis, *p<0.05, **p<0.01, ***p<0.001). **B.** Aortic ring assays showing the number of sprouts from WT and mCTR1$^{KI/KI}$ mice embedded on Matrigel stimulated with VEGF (20 ng/ml) for 9 days. Scale bars=1mm. (two independent experiments were performed using n=5 and n=9 aortic explants from WT and mCtr1$^{KI/KI}$ respectively, compared with One-way ANOVA followed by Tukey's multiple comparisons analysis, **p= 0.001). **C.** Ad.VEGF (1×10^9 pfu) or Ad-LacZ was intradermally injected into the right and left ear skin of WT and mCTR1$^{KI/KI}$ mice, respectively. Ear vasculature (red) was measured by a whole mount staining with CD31 antibody. **D.** Ad.VEGF (1×10^9 pfu) or Ad-LacZ was injected intravitreously into WT and mCTR1$^{KI/KI}$ mice, and retina vasculature was measured by isolectin B4 staining. **C and D**. Histograms show the averaged vessel density. (n=5 samples each for WT and mCTR1$^{KI/KI}$ mice respectively, compared with one-way

ANOVA followed by Tukey's multiple comparisons analysis, **p=0.0059, ****p<0.0001. Data are mean ± SEM). Source numerical data are available in source data.

Author Manuscript Author Manuscript Author Manuscript Author Manuscript

Author Manuscript Author Manuscript Author Manuscript Author Manuscript

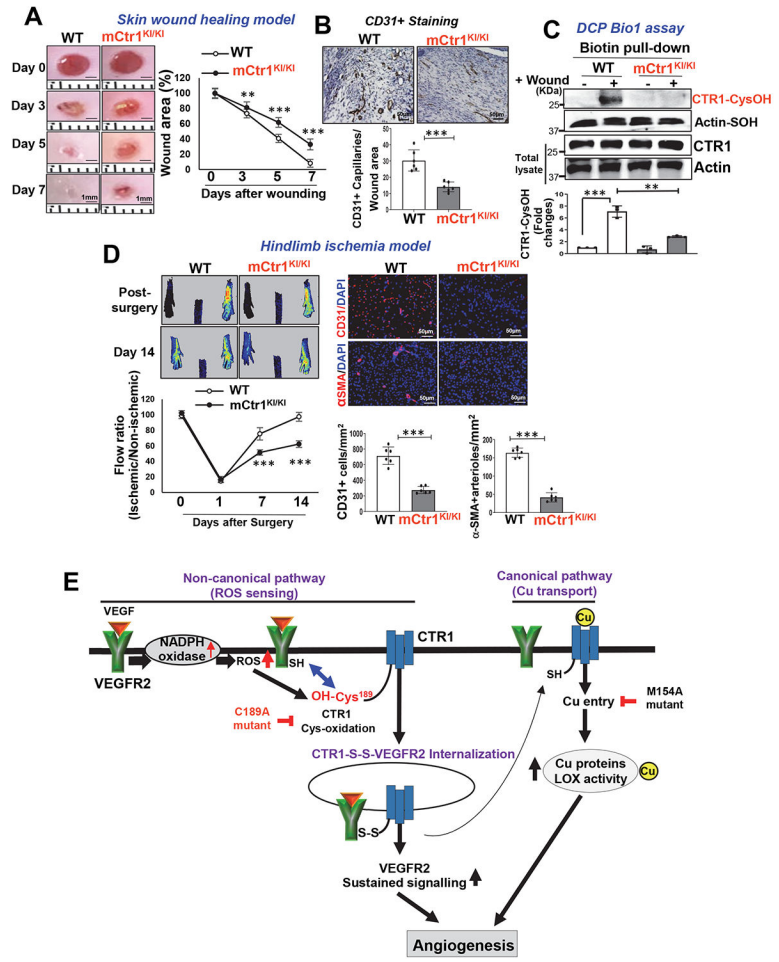

Figure 8: CTR1-CysOH formation is required for reparative angiogenesis *in vivo*.

A, B, C, D. WT and mCTR1$^{KI/KI}$ mice were used for skin wound healing model (**A, B, C**) or hindlimb ischemia model (**D**). In **A**, representative images show time-course for wounded skin closure and graph represents the wound closure rates expressed as % of wound area from control at day 0 after wounding. **B** and **C**. Wounded tissues at day 7 were used to measure CD31^{+} capillary density **(B)** or CysOH formation of CTR1 or actin (control) using DCP-Bio1 assay (**C**). **D.** Left panels show blood flow recovery as determined by the ratio of foot perfusion between ischemic (left) and non-ischemic (right) legs after hindlimb ischemia. Upper panels show representative laser Doppler images and bottom panel shows quantitative analysis. Right panels show the CD31^{+} capillaries or α-SMA^{+} arterioles co-stained with DAPI in ischemic gastrocnemius muscles with quantification. (n=6 mice per group, representative of two independent experiments, compared with two-way ANOVA followed by Bonferroni's multiple comparison analysis (**A** and **D-left panel**), and two-tailed unpaired t-test (**B**, **C**, and **D-right panel)**, *p<0.05, **p<0.01, ***p<0.001. Data are mean ± SEM). Source numerical data and unprocessed blots are available in source data. **E.** Proposed model: VEGF stimulation in ECs rapidly induces CTR1-CysOH formation at Cys^{189} via NOX4-derived ROS, which promotes CTR1-VEGFR2 disulfide bond formation and subsequently their co-internalization to early endosomes driving sustained VEGFR2

Author Manuscript Author Manuscript Author Manuscript Author Manuscript

signaling in a Cu transport-independent manner. Subsequently, internalized CTR1 and VEGFR2 return to the plasma membrane, and which may activate Cu uptake-LOX axis-dependent angiogenic responses. Thus, VEGF-induced CysOH formation of CTR1 at Cys^{189} which promotes Cu entry-*independent* activation of VEGFR2 signaling as well as the canonical Cu entry-*dependent* activation of Cu-dependent enzymes, such as LOX, are orchestrated to enhance developmental and reparative angiogenesis.